LITHOS 468-469 (2024) 107498

Contents lists available at ScienceDirect

LITHOS

journal homepage: www.elsevier.com/locate/lithos

Reaction path model of the formation of abiotic immiscible hydrocarbon fluids in subducted carbonated serpentinites, Lanzo Massif (Western Italian Alps)

Jingyi Huang [a,b,c,*], Dimitri A. Sverjensky [a], Isabelle Daniel [d,e], Alberto Vitale Brovarone [f,g,h]

[a] Dept. of Earth & Planetary Sciences, Johns Hopkins University, Baltimore, MD 21218, United States of America
[b] Dept. of Computer Sciences, University of Idaho, Moscow, ID 83844, United States of America
[c] Earth and Planets Laboratory, Carnegie Institution for Science, Washington, DC 20015, United States of America
[d] Laboratoire de geologie de Lyon - Terre, planètes, environnement, Universite Claude Bernard Lyon1, Villeurbanne 69100, France
[e] Laboratoire de geologie de Lyon - Terre, planètes, environnement, Ecole Normale Supérieure de Lyon, Lyon 69007, France
[f] Dipartimento di Scienze Biologiche, Geologiche e Ambientali, Alma Mater Studiorum, Universit di Bologna, Bologna 40126, Italy
[g] Institut de Minéralogie, de Physique des Matériaux et de Cosmochimie (IMPMC) Sorbonne Université, Muséum National d'Histoire Naturelle, UMR CNRS 7590, IRD, Paris 75005, France
[h] Institute of Geosciences and Earth Resources, National Research Council of Italy, Pisa 56124, Italy

ARTICLE INFO

Keywords:
Abiotic hydrocarbon
Carbonated serpentinites
DEW model
Thermodynamic modeling
Deep carbon fluids

ABSTRACT

Fluids generated from subducted slabs participate in the cycling of deep carbon in the crust and upper mantle. In these fluids, aqueous carbon species vary in oxidation state between +IV and -IV depending on whether the fluids are oxidizing or reducing, respectively. Most studies of subduction-zone fluids have focused on oxidized carbon species. However, recent studies of natural samples have demonstrated the occurrence of deep, reducing fluids, generated in both subducted oceanic upper mantle and crustal rocks. CH_4-H_2-rich fluid inclusions in subducted carbonated serpentinites have demonstrated the existence of abiotic, immiscible, hydrocarbon fluids at upper mantle conditions. To investigate the formation of such immiscible hydrocarbon fluids during the evolution of subducted carbonated serpentinites, we used equilibrium constants from the Deep Earth Water model to carry out predictive chemical mass transfer modeling to simulate the alteration reactions. A novel feature of the models was the inclusion of an immiscible hydrocarbon fluid containing six components ($CH_{4,f}, C_2H_{6,f}, C_3H_{8,f}, isoC_4H_{10,f}$, $CO_{2,f}, H_{2,f}$). This feature enabled prediction of the formation of a separate immiscible fluid in equilibrium with aqueous species and minerals.

We developed a predictive reaction path model of invasive $H_{2,f}$ reacting with carbonated serpentinites and interstitial aqueous fluids for comparison with the natural samples from the Lanzo Massif, western Italian Alps. Over a range of temperatures and pressures, immiscible hydrocarbon fluids formed in association with altered mineral assemblages. Reaction progress caused the transformation of carbonated serpentinites and the formation of clinopyroxene, brucite, graphite, and hydrocarbon fluids, along with changes of *pH*, $logf_{O_2}$, and aqueous species. $CH_{4,f}$ was the most abundant hydrocarbon species in all the models. The overall results at 2.0 GPa and 400 to 450 °C were consistent with the natural samples from the Lanzo Massif. Interestingly, large amounts of H_2O formed due to oxidation of H_2. More hydrocarbons and H_2O formed in models with lower fluid/rock mass ratios or with more reactant H_2. Models at different pressure and temperature conditions showed similar results with some variation in the relative stabilities of aragonite, graphite and olivine solid solution, and associated differences in mineral sequences, hydrocarbon fluids, values of aqueous species, and the final $logf_{O_2}$ and *pH*. Our models strongly support the laboratory and field evidence that reduction of carbonated serpentinites by infiltrating H_2 fluids can cause the formation of immiscible, abiotic hydrocarbon fluids in subduction zones.

* Corresponding author at: Dept. of Earth & Planetary Sciences, Johns Hopkins University, Baltimore, MD 21218, United States of America.
E-mail address: jhuan105@alumni.jh.edu (J. Huang).

https://doi.org/10.1016/j.lithos.2024.107498
Received 25 July 2023; Received in revised form 20 December 2023; Accepted 6 January 2024
Available online 8 January 2024
0024-4937/© 2024 Published by Elsevier B.V.

1. Introduction

It has long been proposed that hydrocarbon fluids could exist in the deep Earth (Kolesnikov et al., 2009, 2017; Kudryavtsev, 1959; Kutcherov and Krayushkin, 2010; Mendeleev, 1877). Although controversial (McCollom, 2013; Sephton and Hazen, 2013), a deep, abiotic theory for the origin of hydrocarbons received support in the late 20th century from the hypothesis of a deep hot biosphere feed by ascending abiotic fluid hydrocarbons from the deep Earth (Gold, 1992, 2001; Kudryavtsev, 1951). However, the amounts of abiotic hydrocarbons that could be produced in the upper mantle were never quantified and remain highly speculative.

Recent studies have suggested evidence of possible abiotic hydrocarbon-H_2-bearing fluids in association with ultramafic or mafic rocks and serpentinization in mid-ocean ridge settings where the hydrocarbons are present in minor quantities dissolved in the circulating aqueous fluids (Alt et al., 2013; Klein et al., 2019; McDermott et al., 2015; Proskurowski et al., 2008). However, it is doubtful that the CH_4 formed recently in the present hydrothermal circulation systems (McDermott et al., 2015; Reeves and Fiebig, 2020). For example, Klein et al. (2019) suggested that H_2 and CH_4 can be formed inside olivine-hosted aqueous fluids as a result of host-inclusion interactions during cooling and subsequently released into the mid-ocean ridge hydrothermal circulation system.

Many fewer studies have been concerned with hydrocarbon production during high-pressure metamorphism in subduction zones, where most studies have typically focused on oxidized carbon species dissolved in the fluid phases (Dasgupta and Hirschmann, 2010; Hacker et al., 2003; Scambelluri et al., 2019). Subduction zone serpentinization has been proposed to produce large amounts of H_2 and CH_4 (Boutier et al., 2023; Vitale Brovarone et al., 2020). Additionally, CH_4 has been found in high-pressure and ultra-high-pressure rocks (Tao et al., 2018; Wang et al., 2022; Zhu et al., 2020). Experimental and theoretical studies have demonstrated that H_2 and light hydrocarbons can be immiscible at subduction zone conditions (Huang et al., 2017; Huang et al., 2023; Li, 2017; Pruteanu et al., 2017). However, the generation of reduced-carbon species in subduction zone fluids or as immiscible phases has not received much attention. Nevertheless, natural confirmation of immiscible, CH_4-H_2-bearing fluids related to serpentinization in subduction zones have now been found world-wide. For example, coexisting aqueous and $CH_4 - H_2$-rich gaseous fluid inclusions in the Lanzo massif, western Italian Alps (Giuntoli et al., 2020; Pelletier and Müntener, 2006; Sverjensky et al., 2020; Vitale Brovarone et al., 2017, 2020) have been suggested to document immiscibility of reduced fluids in metamorphic fluids. In these rocks, CH_4 formed by H_2-mediated reduction of carbonate in carbonated serpentinites. The reaction also resulted in the formation of diopside, brucite, graphite, ±Ca-rich garnet (Giuntoli et al., 2020; Vitale Brovarone et al., 2017). A recent geochronological study indicates that the event of CH_4 formation happened at peak metamorphic conditions (Piccoli et al., 2023), corresponding to about 500 °C and depths up to 80 km, or ~ 2.5 GPa (Vitale Brovarone et al., 2017 and references therein).

In addition to natural examples of abiotic hydrocarbons, numerous experimental studies of abiotic hydrocarbon formation at elevated temperatures and pressures have been reported (Foustoukos and Stern, 2012; Manning et al., 2013; McCollom, 2013). Under crustal conditions, the formation of hydrocarbons in serpentinization experiments has been widely studied with and without catalysts such as metallic iron (Barbier et al., 2020). At higher, upper mantle pressures, some experimental studies have focused on fluids without minerals present. For example, immiscible $CH_4 - C_2H_6 - H_2$ fluid inclusions were recorded in quartz at 1.5–2.5 GPa and 600–700 °C (Li, 2017), and immiscible hydrocarbon droplets containing isobutane and other hydrocarbons were observed with in situ Raman spectroscopy at 1.6–4.6 GPa and 300 °C (Huang et al., 2017; Huang et al., 2023). Other experiments at elevated temperatures and pressures have reacted iron and iron minerals with aqueous fluids and carbonates (Mukhina et al., 2017).

Overall, natural examples and experiments at upper mantle temperatures and pressures indicate that the formation of immiscible abiotic hydrocarbons does occur. However, quantitative, predictive models of the formation of immiscible abiotic hydrocarbon fluids in geologic settings at depth have been lacking. In this study, we conducted predictive, irreversible chemical mass transfer modeling to simulate the formation of hydrocarbon fluids in a well-documented natural setting. We chose to model the reduction of carbonated serpentinites and the associated production of an immiscible CH_4-rich fluid in the Lanzo Massif previously described in detail by Vitale Brovarone et al. (2017). Following the genetic model by Vitale Brovarone et al. (2017), we modeled the interaction between H_2-rich fluids and carbonated serpentinites in the pressure and temperature range of 1.0–2.0 GPa and 400–500 °C which is consistent with reported subduction zone conditions (Holt and Condit, 2021; Penniston-Dorland et al., 2015; Syracuse et al., 2010; Van Keken et al., 2002). Our models provide a test of our ability to predict the formation of immiscible hydrocarbon fluids in a chemically and mineralogically complex system at elevated pressure-temperature conditions for comparison with the observed mineral assemblages and fluid inclusion compositions previously described for the reduced carbonated serpentinites from the Lanzo Massif.

2. Geologic setting of the Lanzo Massif and abiotic methanogenesis during the reduction of carbonated serpentinites

The ultramafic rocks of the Lanzo Massif in the western Italian Alps underwent Cenozoic eclogite-facies peak metamorphic conditions to about 500–550 °C and 2 GPa (Pelletier and Müntener, 2006; Rubatto and Hermann, 2001). The massif includes carbonated serpentinites, regarded as the products of sub-seafloor hydrothermal reactions (Lagabrielle et al., 1990; Pelletier and Müntener, 2006; Rubatto and Hermann, 2001; Vitale Brovarone et al., 2017). The carbonated serpentinites are located in the pervasive serpentinized shell outside the peridotite core of the massif. The shell surrounds mostly the north and west sides of the peridotite core. For the purposes of the present study, the detailed petrographic, fluid inclusion, isotopic, modeling, and geochronological results reported by Vitale Brovarone et al. (2017), Giuntoli et al. (2020), and Piccoli et al. (2023).

can be summarized by the following key points relevant to our reaction path modeling:

- The samples of carbonated serpentinite consist of clasts of serpentinite embedded in a Ca-carbonate matrix.
- Pristine serpentinite clasts consist mainly of antigorite – the serpentine mineral stable at high temperature and pressure conditions – and small amounts of chlorite and magnetite.
- The reacted serpentinite clasts are coated by ubiquitous graphite rims. Other product minerals include diopside ± brucite ± Ca-rich garnet ± perovskite ($CaTiO_3$).
- The reacted rocks are found along discrete layers within the carbonated serpentinite, which were interpreted as fluid pathways and shear zones (Giuntoli et al., 2020). Overall, the degree of alteration of the serpentinite clasts is highly variable on a spatial scale of meters.
- Petrographic relations indicate that graphite formation occurred at high-pressure conditions in the antigorite stability field. Dating of *syn*-reduction perovskite including CH_4 and graphite inclusions provided an age of 49.6 ± 1 Ma (Piccoli et al., 2023), which is consistent with previous constraints on the peak metamorphic age of the Lanzo massif (Rubatto and Hermann, 2001).
- Two types of structurally coexisting fluid inclusion populations were found in the carbonate matrix adjacent to serpentinite clasts and the reacted rims of serpentinite: a $CH_4 - H_2$-rich population and a H_2O-rich population. These two populations were interpreted to

represent coexisting immiscible fluids (Sverjensky et al., 2020; Vitale Brovarone et al., 2017).

- The $\delta^{13}C$ values of the residual, reacted carbonate samples are up to about 8 per mil heavier than the least reacted samples which have typical marine carbonate values of about 2–3 per mil relative to the PeeDee Belemnite standard (Vitale Brovarone et al., 2017). These values are consistent with the partial transformation of carbonate into CH_4.
- The CH_4 genesis was interpreted as the result of H_2-carbonate interactions along channelized fluid pathways inside the carbonated serpentinite. The process was summarized according to the following overall reaction:

$$antigorite + 17Ca - carbonate + 68H_2 = 17diopside + 31brucite + 17CH_4 + 34H_2O \quad (1)$$

$$2Mg_{24}Si_{17}O_{42.5}(OH)_{31} + 17CaCO_3 + 68H_2 = 17CaMgSi_2O_6 + 31Mg(OH)_2 + 17CH_4 + 34H_2O \quad (2)$$

n. b. here we use the formula of antigorite as documented in the thermodynamic database of Berman (1988) which was the source of the standard state thermodynamic properties of minerals in our study.

- Overall, the mineral assemblages and fluid inclusions suggest the reduction of carbon in Ca-carbonate by the H_2-fluids to form CH_4 and graphite. Reaction between the external H_2 and the newly formed graphite was also proposed to generate additional CH_4.
- The pressure and temperature conditions of the reactions were determined by the presence of graphite and aragonite inclusions in magnetite, and *syn*-reduction antigorite, and modeled in a simplified $Ca-Mg-Si-C-O-H$ thermodynamic system. The minimum condition was inferred to be 1.0 GPa and 370°C (i.e., 370 $^\circ C\ GPa^{-1}$ of gradient, same as below) constrained by graphite-aragonite coexistence along the exhumation path of the Lanzo massif. The maximum condition was predicted to be about 2.5 GPa and 500 °C (200 $^\circ C\ GPa^{-1}$) constrained by the peak metamorphic condition of the Lanzo Massif.
- The oxygen fugacities during the reactions were estimated to range from $logf_{O_2}$ -29 to −37 (QFM −3 to −6), assuming graphite saturation and the co-occurrence of magnetite in the carbonated serpentinites.

3. Methods

3.1. Thermodynamic data for aqueous species and minerals

We have used the geochemical Deep Earth Water (DEW) model which was built to address the predictive geochemical modeling challenge of a huge range of temperatures, pressures, and chemically complex systems (Huang and Sverjensky, 2019; Sverjensky, 2019; Sverjensky et al., 2014). The DEW model is based on predictive geochemical theory resting on decades of theoretical and experimental studies of the thermodynamic properties of electrolytes, neutral aqueous solutes, metal-complexes, and organic species (Sverjensky, 2019). The DEW model enables prediction of equilibrium constants involving aqueous species of all types to be incorporated into the data files for aqueous speciation, solubility, and chemical mass transfer codes. Here we use the codes EQ3 & EQ6 (Wolery, 1992) modified to operate at elevated temperatures and pressures. The standard Gibbs free energies of formation of the end-member mineral components were calculated with the modified Berman thermodynamic database (Berman, 1988; Sverjensky, 2019; Sverjensky et al., 1991).

3.2. Standard Gibbs free energies of fluid H_2 and CO_2

The calculation of chemical mass transfer involving immiscible hydrocarbon fluids requires the computation of standard Gibbs free energies of the pure end-member hydrocarbon species as well as other pure fluid species that are relevant to the modeling described below. Here we made use of six organic and inorganic pure fluid species, all of which are relevant to this study. These fluid species include the following: methane ($CH_{4,f}$), ethane ($C_2H_{6,f}$), propane ($C_3H_{8,f}$), isobutane ($isoC_4H_{10,f}$), carbon dioxide ($CO_{2,f}$), and hydrogen ($H_{2,f}$) where the subscript f refers to the supercritical fluid compound. The apparent standard Gibbs free energies of formation ($\Delta G^0_{f;T,P}$) of these species are given in the Appendix A. They were obtained by first calculating the $\Delta G^0_{f;T,P^0}$ of the pure gas, then the fugacity coefficients (ϕ) were obtained from the GFluids spreadsheet (Zhang and Duan, 2010) at 1.0–5.0 GPa and 400–650 °C. As the GFluids model was not usable below 400 °C, values of the fugacity coefficients at 300–400 °C were obtained by empirical extrapolation from the higher temperatures. Equilibrium constants involving these species and aqueous species were calculated using the DEW model and incorporated into the data files for the codes EQ3 and EQ6.

3.3. Incorporation of immiscible hydrocarbon fluids in aqueous speciation, solubility, and chemical mass transfer models

Although aqueous C-species of many types in the spectrum of inorganic to organic species have long been used in aqueous speciation, solubility, and chemical mass transfer models, immiscible inorganic or organic fluids have not been used in such models. Here, we incorporated such species using a number of approximations. Mathematically, this incorporation can be done by including the predicted *logK* values for equilibrium between any potentially immiscible fluid species (e.g. $H_{2,f}$ or $CH_{4,f}$) and a strict basis species into the thermodynamic data file as a "mineral species". For example, we decided to put fluid methane ($CH_{4,f}$) into the datafile of EQ3 and EQ6 using the equilibrium

$$CH_{4,f} + 2O_{2,g} = CO_3^{2-} + 2H^+ + H_2O \quad (3)$$

During model calculations, the above equilibrium enables the fluid species to reach saturation and "precipitate" as a pure fluid phase immiscible with the aqueous fluid and any minerals in equilibrium with the aqueous fluid according to the reaction

$$CH^0_{4,aq} = CH_{4,f} \quad (4)$$

Examples of reactions such as Eq. (4), which are just solubility reactions, are discussed below as functions of temperature and pressure.

Building on the above, two or more such potentially immiscible fluid species can be entered as potential components of a "solid-solution" in the data file of the codes EQ3 and EQ6, which enables formation of an immiscible fluid phase (e.g., a hydrocarbon fluid phase containing multiple hydrocarbon components). In the present study, the end-member components of the immiscible hydrocarbon fluid were assumed to mix ideally. At elevated temperatures and pressures, this is a major assumption. However, in almost all our model results the hydrocarbon fluid that formed was >90% fluid CH_4. Therefore, as a first approximation, it seems reasonable to assume ideal mixing in the hydrocarbon fluid.

3.4. Conceptual model and assumptions for chemical mass transfer calculations

As discussed above, the carbonated serpentinite of interest consisted of clasts of serpentinite embedded in an aragonite matrix. The serpentinite is composed mainly of antigorite with minor magnetite and chlorite. We assume here a conceptual model in which an external H_2 fluid invades and reacts with the carbonated serpentinite assemblages that contain some interstitial aqueous fluid. As a first approximation, the composition of this initial interstitial fluid was assumed to be determined by equilibrium with the rock minerals. Using the aqueous

speciation and solubility code EQ3 (Wolery, 1992), the concentrations of the elements Ca, Si, Fe, and Al, were determined by equilibrium with aragonite, antigorite, magnetite, and the clinochlore component of a chlorite solid solution (X_{Mg} 0.97), respectively. Mg was set to a value below the saturation of brucite. Na and Cl were set to low values of 0.001 m as the salinity of the aqueous fluid predating the reactions is not known. C was set to a small value, e.g. $\leq$ 0.1 m, in equilibrium with aragonite, so the amount of aqueous C is not important in the initial fluid. Either Na^+ or H^+ was determined by charge balance leading to a calculated value of the *pH*. Wide ranges of the initial value of the $logf_{O_2}$ were tested. Optimal values were selected based on the constraints of minimizing the initial aqueous carbon concentration in equilibrium with aragonite such that the computed aqueous Ca concentrations were not so high as to result in supersaturation of the initial fluid with respect to diopside or clinopyroxene solid solution. These constraints typically resulted in $logf_{O_2}$ values of QFM to QFM - 2. As an example, the bulk composition and most abundant C-species and fluid properties of an initial fluid at 400 °C and 2.0 GPa are listed in Table 1 where it can be seen that the $logf_{O_2}$ is equal to QFM-1.3.

The initial aqueous fluids were subsequently used as input to the chemical mass transfer code (EQ6), together with the carbonated serpentinite reactant minerals and external H_2 fluid reactant. The Lanzo carbonated serpentinite was approximated by 15 vol% of aragonite and 85 vol% of serpentinite. The serpentinite contained 96.5 vol% of antigorite, 1.0 vol% of magnetite, and 2.5 vol% of chlorite. The volume percentages refer throughout to the formulae and volumes in the Berman (1988) database at ambient temperature and pressure. The abundances of the minerals in the carbonated serpentinite and the serpentinite itself cited above provide a standard example for our models. Additional models were considered for higher aragonite/serpentinite ratios (Appendix A). To explore the effect of variable fluid-rock (F/R) ratio, the total amount of reactant rocks was varied from 1590 g to 10,000 g per 1000 g of H_2O in the initial aqueous fluid. The initial amount of reactant H_2 in moles per 1000 g of H_2O was determined by the need to overwhelm the redox buffering capacity of the initial rock in order to form hydrocarbon fluid. Within the framework of the assumptions adopted above, numerous reaction path models were run to explore variable temperatures, pressures, initial oxidation states, and F/R ratios. A representative set of these is included in the Supplementary Materials. The overall goal was to compare the predicted model outputs to the mineral assemblages in the rocks and the hydrocarbon fluids recorded in fluid inclusions reported for the Lanzo Massif by Vitale Brovarone et al. (2017) and Giuntoli et al. (2020).

Table 1
Summary of the initial and final fluid compositions and mineral assemblages at 400 °C and 2.0 GPa with F/R 0.1. Full details of the aqueous speciation of all the elements at each step of the reaction progress are given in the reaction path output file (see File 1 in Appendix A).

INITIAL	Parameter		FINAL	Parameter
FLUID	value[a.]		FLUID	value[a.]
Na	0.001		*Na*	0.0006
Mg	0.8		*Mg*	0.969
Ca	0.028		*Ca*	0.031
Fe	0.003		*Fe*	0.001
Al	0.00002		*Al*	0.00002
Si	0.003		*Si*	0.002
Cl	0.001		*Cl*	0.0006
C	0.05		*C*	2.413
$CH_{4,aq}$	0.0314		$CH_{4,aq}$	2.408
HCO_3^-	0.0038		HCO_3^-	9e-7
$Ca(HCO_3)^+$	0.0067		$Ca(HCO_3)^+$	2e-6
CO_3^{2-}	0.0002		CO_3^{2-}	6e-8
$CaCO_{3,aq}$	0.0013		$CaCO_{3,aq}$	6e-7
$H_2CO_{3,aq}$	0.0003		$H_2CO_{3,aq}$	6e-8
$CO_{2,aq}$	0.0004		$CO_{2,aq}$	8e-8
$HCOO^-$	0.0011		$HCOO^-$	7e-6
$Fe(HCOO)^+$	0.0024		$Fe(HCOO)^+$	0.00005
$Ca(HCOO)^+$	0.0016		$Ca(HCOO)^+$	0.00001
pH	5.64		*pH*	5.77
Neutral *pH*	3.60		Neutral *pH*	3.60
$logf_{O_2}$	−27.4		$logf_{O_2}$	−30.2
ΔQFM	−1.3		ΔQFM	−4.1
REACTANT MINERALS	COMPONENTS	REACTANT MOLE FRACTION	FINAL PRODUCT MOLE FRACTION	FINAL PRODUCT MOLES
ARAGONITE	$CaCO_3$	1.0	n.d.	0.0
ANTIGORITE	$Mg_{24}Si_{17}O_{73.5}H_{31}$	1.0	1.0	1.598
MAGNETITE	Fe_3O_4	1.0	1.0	0.113
CHLORITE	Clinochlore	0.97	0.90	1.696
	Chamosite	0.03	0.10	0.188
PRODUCT MINERALS	COMPONENTS			
CLINOPYROXENE	Diopside	n.d.	0.90	14.786
	Hedenbergite	n.d.	0.10	1.643
	Jadeite	n.d.	0.0	0.0
BRUCITE	$Mg(OH)_2$	n.d.	1.0	31.053
GRAPHITE	*C*	n.d.	n.d.	0.0

[a.]Concentrations given in molality (m).

4. Results

4.1. Predicted equilibria between fluid hydrocarbons, aqueous C-species, and graphite at upper mantle conditions

4.1.1. Predicted equilibria between pure immiscible fluids and aqueous species

Both H_2O-bearing and $CH_4 - H_2$ fluids were observed in microstructurally coexisting fluid inclusions populations of the Lanzo reduced carbonated serpentinite, suggesting at least two types of immiscible fluids could appear in the natural samples. Accordingly, a number of fluid phases, including hydrocarbon and inorganic species at upper mantle conditions were incorporated in our model. The values of the equilibrium constants were predicted using the DEW model (Sverjensky et al., 2014) adapted for equilibria between pure fluid and aqueous species. The standard states for the fluid species $CH_{4,f}$, $C_2H_{6,f}$, $CO_{2,f}$, and $H_{2,f}$ were chosen to be the pure fluids at the temperatures and pressures of interest. Equilibria between such fluids and the corresponding aqueous species represent the maximum activities of the aqueous species, i.e. the solubility of the pure fluid component as an aqueous species.

The predicted *logK* values displayed in Figs. 1A - D cover a wide range of temperatures and pressures from 300–650 °C and 0.5–5.0 GPa. It can be seen in the figures that, overall, the *logK* values increased with temperature and decreased with pressure, with some exceptions at 0.5–1.0 GPa. In other words, the solubilities of fluid $CH_{4,f}$, $C_2H_{6,f}$, $CO_{2,f}$, and $H_{2,f}$ in aqueous solutions increase with temperature but decrease with pressures greater than about 1.5 GPa. At temperatures between 400 and 500 °C, the solubilities decrease in the order: $CH_4 < C_2H_6 < H_2 < CO_2$. As a first order generalization, it should therefore be easier to form immiscible CH_4-rich fluids than any of the others.

Although the equilibria shown in Figs. 1A-D are fundamental to the formation of immiscible fluids, other factors also may exert a strong influence. Clearly, the redox state of a system is extremely important. For example, if the $logf_{O_2}$ is low enough, the formation of a CH_4-rich

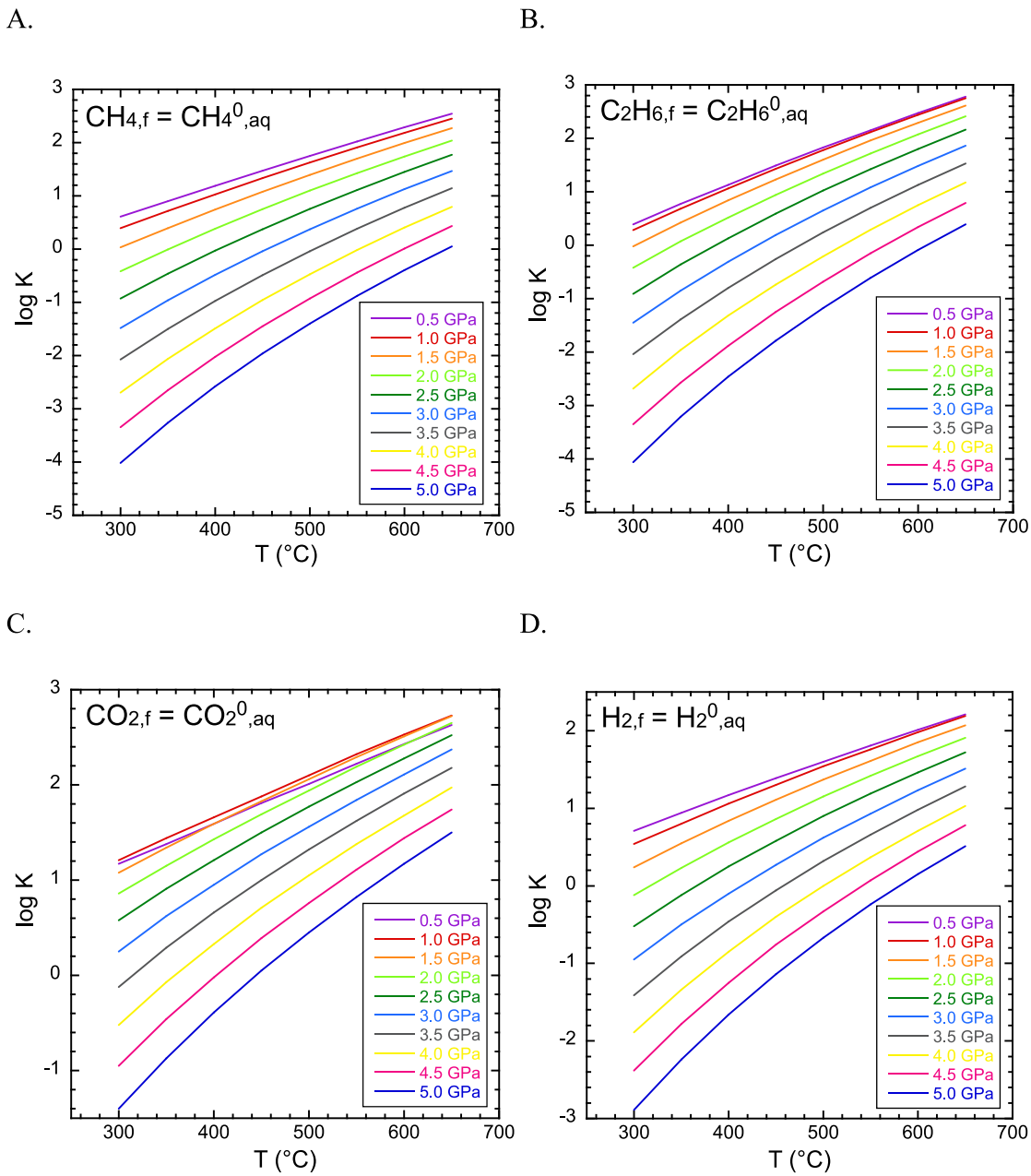

Fig. 1. *Log K* of reactions of fluid species and aqueous species. (A) CH_4, (B) C_2H_6, (C) CO_2, and (D) H_2.

fluid will be strongly favored relative to the other C-species. This tendency can be expected to be magnified when the H_2 is continuously added and reacted with minerals. Furthermore, the equilibria between aqueous and fluid species depend on $logf_{O_2}$, pH, total C content and other features of the system. Different results could occur with a wider range of conditions beyond the scope of this work.

4.1.2. *Predicted equilibria between pure fluid methane, aqueous methane, and graphite*

Graphite was an important product in the Lanzo reduced carbonated serpentinite and was observed to be closely related to the $CH_4 - H_2$ fluid inclusions (Vitale Brovarone et al., 2017). In Fig. 2, the stability fields of aqueous CH_4, pure fluid CH_4 ($CH_{4,f}$) and graphite were plotted as functions of $logf_{O_2}$ and $loga_{CH^0_{4,aq}}$ at 1.0–2.0 GPa and 400–500 °C (Fig. 2). The equilibrium between aqueous and fluid CH_4 is determined solely by the equilibrium in Fig. 1A. It can be seen that the predicted $loga_{CH^0_{4,aq}}$ in equilibrium with $CH_{4,f}$ range from 0.4 to 1.1 in Figs. 2A -D. The activity coefficient of $loga_{CH^0_{4,aq}}$ was assumed to be unity in our subsequent modeling. As expected from Fig. 1A, the stability field of $CH_{4,f}$ expanded against $CH^0_{4,aq}$ at lower temperature and higher pressure.

The equilibrium between fluid $CH_{4,f}$ and graphite can be expressed in terms of $logf_{O_2}$ by writing the reaction

$$Graphite + 2H_2O = O_{2,g} + CH^0_{4,aq} \quad (5)$$

From which the $logf_{O_2}$ can be expressed by the $logK$ of Eq. (5) and $log\, a_{CH^0_{4,aq}}$ as

$$logf_{O_2} = -loga_{CH^0_{4,aq}} + logK \quad (6)$$

assuming that a_{H_2O} is unity. In Figs. 2A - D, this equilibrium is expressed as a line with a slope of −1.0 and intersecting the line representing equilibrium between $CH_{4,f}$ and $CH^0_{4,aq}$ at an invariant point. It can also be seen that the equilibrium between fluid CH_4 and graphite is about 3.0 log units below the QFM buffer, in agreement with the prediction by Vitale Brovarone et al. (2017). We also included the magnetite-α-Fe buffer, and the $H_2O - H_{2,f}$ buffers with $a_{H_{2,f}}$ of 0.1 and 1.0. These buffers

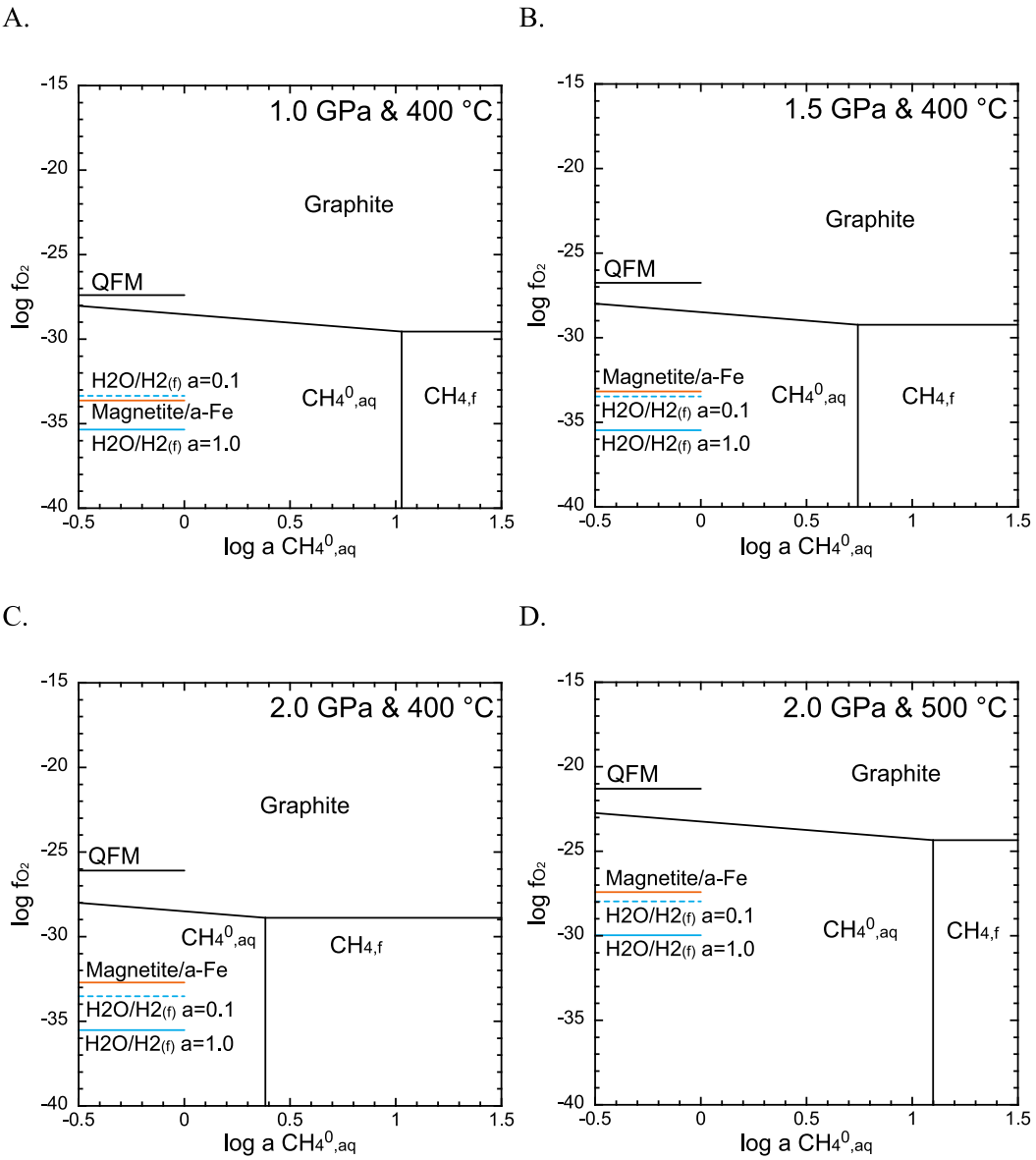

Fig. 2. $Logf_{O_2}$ vs. $loga_{CH^0_{4,aq}}$ diagrams of the stability field among graphite, $CH^0_{4,aq}$, and $CH_{4,f}$ at (A) 1.0 GPa & 400 °C, (B) 1.5 GPa & 400 °C, (C) 2.0 GPa & 400 °C, and (D) 2.0 GPa & 500 °C.

all plot in the $CH_{4,aq}$ and $CH_{4,f}$ fields.

The phase diagrams in Figs. 2A - D provided guidance for setting up the initial $logf_{O_2}$ of our model aqueous fluid resulting in values above the $CH^0_{4,aq}$ field and amounts of initial carbon lower than saturation with graphite or $CH_{4,f}$. Starting from these conditions, when $logf_{O_2}$ decreases, and when $CH^0_{4,aq}$ increases, the figures show that it can be expected that the boundary of $CH^0_{4,aq}$ and $CH_{4,f}$ will be reached, followed by the stability field of CH_4-rich hydrocarbon fluid.

It should be noted here that although graphite appears as a phase in Figs. 2A - D, these figures refer to a chemical system without the component CaO, an important component in the natural carbonated serpentinites. When CaO is included, the stability of graphite is limited

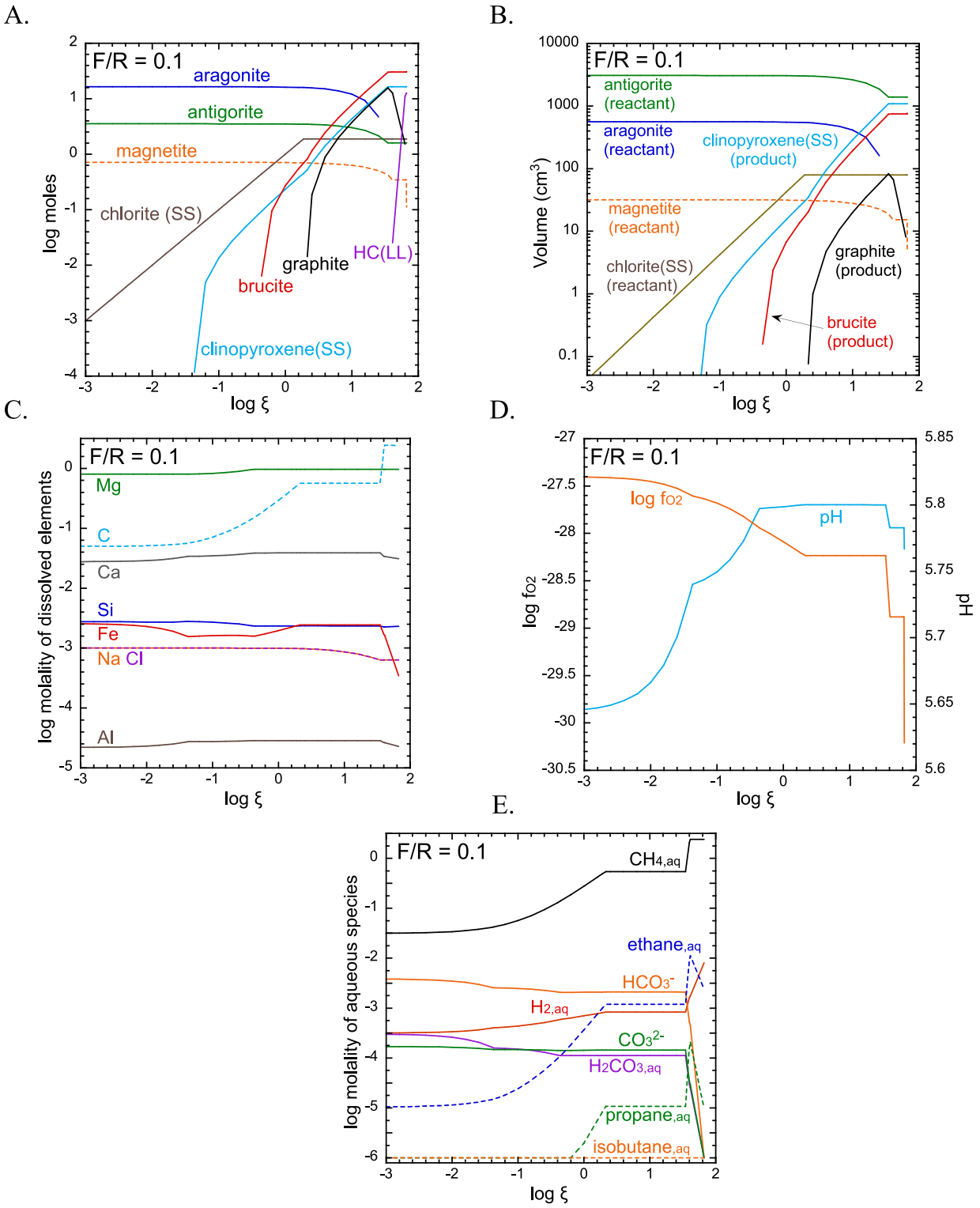

Fig. 3. Reaction path model of the reduction of carbonated serpentinite by H_2 at 2.0 GPa and 400.0 °C with F/R equal to 0.1 (by weight) as a function of the logarithm of the reaction progress ($log\ \xi$): (A) minerals and hydrocarbon fluid, (B) volumes of minerals, (C) dissolved elements, (D) $logf_{O_2}$ and pH, and (E) aqueous species.

by the appearance of aragonite or calcite solid solution, depending on the value of the $log\left(a_{Ca^{2+}}/(a_{H^+})^2\right)$ in the aqueous phase. For the conditions we modeled below, the stability field of graphite is replaced by aragonite or calcite solid solution at 1.0 GPa and 400 °C.

4.2. Fluid hydrocarbon formation during the destruction of carbonated serpentinites in the Lanzo Massif

Chemical mass transfer models of the transformation of carbonated serpentinites by H_2 fluids were conducted at 1.0–2.0 GPa and 400 °C–500 °C consistent with the conditions proposed for the Lanzo Massif (Vitale Brovarone et al., 2017). The initial aqueous fluids were predicted at each pressure and temperature condition (Table 1, S-1, S-2, S-3, S-4) using an aqueous speciation solubility model as described above (section 3.3). The initial total concentrations of the aqueous carbon were 0.01, 0.05, or 0.1 m, which were the lowest values usable given our assumptions about equilibrium with the minerals and with initial $logf_{O_2}$ values between QFM −1.6 to +1.2. The saturation activity of $CH^0_{4,aq}$ increased with temperature at the same pressure. The carbon speciation in the initial fluids was controlled by $logf_{O_2}$ relative to the QFM buffer and the total aqueous carbon concentrations. For example, at 1.5 GPa and 400 °C, two oxidation states could be considered: at $logf_{O_2}$ of QFM + 1.0, $CH_{4,aq}$ is 0.03% of the total carbon of 0.01 m, whereas at $logf_{O_2}$ of QFM–1.4, $CH_{4,aq}$ is 91.4% of the total carbon of 0.1 m. Importantly, the different oxidation states of these two fluids did not affect the major results of the mass transfer reactions. Therefore, either fluid could be used at each pressure and temperature. In other words, the initial values of $logf_{O_2}$ in the fluid were not important variables. The main reason being that in all cases the total initial carbon in the fluid was low.

4.2.1. The standard model at 2.0 GPa and 400.0 °C and F/R (fluid/rock by weight) equal to 0.1

Here we present a mass transfer model at 2.0 GPa and 400 °C and F/R equal to 0.1 that can serve as a representative example of our modeling (Table 1, Fig. 3). At this temperature and pressure, the activity of $CH^0_{4,aq}$ in equilibrium with pure methane fluid was 2.4 (see Fig. 1A). Therefore, as the aqueous activity coefficient in our model for neutral species was assumed to be unity, at least 2.4 m $CH^0_{4,aq}$ would need to accumulate in the fluid during the mass transfer reactions for an immiscible pure methane fluid to form. In our models, a hydrocarbon fluid with variable composition could form. Such a fluid was more stable than a pure methane fluid; therefore, it could form at concentrations of C <2.4 m. The initial mineral reactants were 16.45 mol of aragonite, 3.53 mol of antigorite, 0.71 mol of magnetite, and 1.88 mol of chlorite(ss) per 1000 g of H_2O. The initial aqueous fluid/rock (F/R) mass ratio was 0.10. This ratio was the lowest value tested and corresponded to 10.0 kg of rock and of a dilute initial aqueous fluid containing 1.0 kg of H_2O. The endpoint of the model was determined by the initial amount of H_2 with a value of 66.5 mol per 1000 g of H_2O (Table 2). This value of H_2 resulted in the formation of hydrocarbon fluids without secondary olivine(ss) appearance due to the reduction of magnetite.

Table 2
The amounts of initial reactant H_2, and the initial and final rock and fluid-rock (F/R) mass ratios, as well as the final excess of H_2O created and the amounts of immiscible hydrocarbon fluid created.

Reactants				Final			
F/R	M_R [a]	N_{H_2} [b]	H_2/R [c]	$M_R{}'$ [a]	F/R'	Extra N_{H_2O} [d]	N_{HC} [e]
0.10	10.0	66.5	0.0133	9.27	0.17	32.3	12.7
0.20	5.00	33.2	0.0133	4.63	0.28	16.5	5.15
0.33	3.03	20.2	0.0133	2.81	0.42	10.3	2.20
0.63	1.59	10.6	0.0133	1.46	0.75	5.57	0.012

[a]mass of rock in kg, [b]moles of H_2, [c]mass ratio of H_2 and rock, [d]Excess moles of water created relative to the initial 55.51 mol, [e]moles of hydrocarbon fluid created.

The initial and final aqueous fluid compositions and mineral assemblages are shown in Table 1 and the detailed mass transfer results are shown as a function of the logarithm of the reaction progress ($log\ \xi$) in Figs. 3A–E. Here, ξ represents the number of moles of H_2 added. The full reaction path output file is given in Appendix A. It can be seen in Fig. 3A that the reactant minerals, aragonite, antigorite, and magnetite were stable in the beginning, as these were used in the EQ3 code to develop the initial aqueous fluid chemistry, while chlorite(ss) increased with $log\ \xi$. At a $log\ \xi$ value of −1.37, clinopyroxene(ss) appeared consisting of almost pure diopside (95%) and minor hedenbergite (5%). The mole fraction of diopside decreased slightly to 90% until the end of the reaction (Table 1). Chlorite(ss) reached a plateau after $log\ \xi$ of 0.28 because it contains all the aluminum in the system. Shortly after, brucite started to form, then antigorite and aragonite decreased strongly. Graphite then formed and increased until aragonite was totally destroyed; meanwhile, antigorite stopped decreasing. The graphitization could be expressed as the following reaction:

$$antigorite + 17Ca - carbonate + 34H_2 = 17diopside + 31brucite + 17graphite \quad (7)$$

$$Mg_{48}Si_{34}O_{85}(OH)_{62} + 17CaCO_3 + 34H_2 = 17CaMgSi_2O_6 + 31Mg(OH)_2 + 17C + 34H_2O \quad (8)$$

Finally, hydrocarbon fluid formed and completed replaced graphite. This reaction could be expressed as the reaction below:

$$graphite + 2H_{2,f} \rightarrow CH_{4,f} \quad (9)$$

The overall reaction of methane genesis was presented in Eqs. (1 and 2). The hydrocarbon fluid contained almost pure $CH_{4,f}$ (99.7%), as well as $C_2H_{6,f}$ (0.1%), $H_{2,f}$ (0.2%). Only trace amounts of $C_3H_{8,f}$ and $isoC_4H_{10,f}$ were produced. The amount of hydrocarbon fluid increased mainly during the final period of reaction progress ($\Delta log\ \xi$ 0.21).

The change of mineral volumes can be seen in Fig. 3B. The volumes shown refer to 25 °C and 0.1 MPa but these differ by less than about 3% from the volumes at 400 °C and 2.0 GPa. For the model system volume of in a 4600 cm^3 (3800 cm^3 of reactant rock and 800 cm^3 of initial aqueous fluid), the volumes show a dramatic destruction of antigorite and aragonite by about 1680 cm^3 and 560 cm^3, respectively, while the other two reactants (magnetite and chlorite) were just accessory minerals. In terms of product minerals, about ~ 1090 cm^3 of clinopyroxene(ss) and ~ 770 $cm^3$of brucite were generated. Despite the significant number of moles of graphite formed, the volume of graphite is small. The total volume of product minerals was about ~ 380 cm^3 less than the destroyed reactants. However, in addition to the mineral products, about 32.3 mol of H_2O and 12.7 mol of fluid CH_4 were also produced (Table 2), which corresponded to about 487 cm^3 of H_2O and 332 cm^3 of fluid CH_4, respectively (see also Fig. 4B below). Overall, the volume of the system expanded by around 440 cm^3. The reactions are self-promoting because more fluid CH_4 formed at 2.0 GPa and 400 °C than lower pressures (see section 4.2.3).

The molalities of most dissolved elements, except C and $H_{2,aq}$, showed only small changes as a function of $log\ \xi$ (Fig. 3C). Ca increased slowly and then decreased a little in the end. Fe decreased because of the formation of clinopyroxene(ss). Then after clinopyroxene(ss) reached a peak, the reduction of magnetite caused the decrease of Fe. Na, Cl, and Al did not participate significantly in any reactions. However, the total dissolved C increased strongly with $log\ \xi$ as aragonite progressively dissolved. Methane formed initially by reaction of $H_{2,aq}$ with aragonite. Once graphite appeared, the equilibrium between it and the remaining

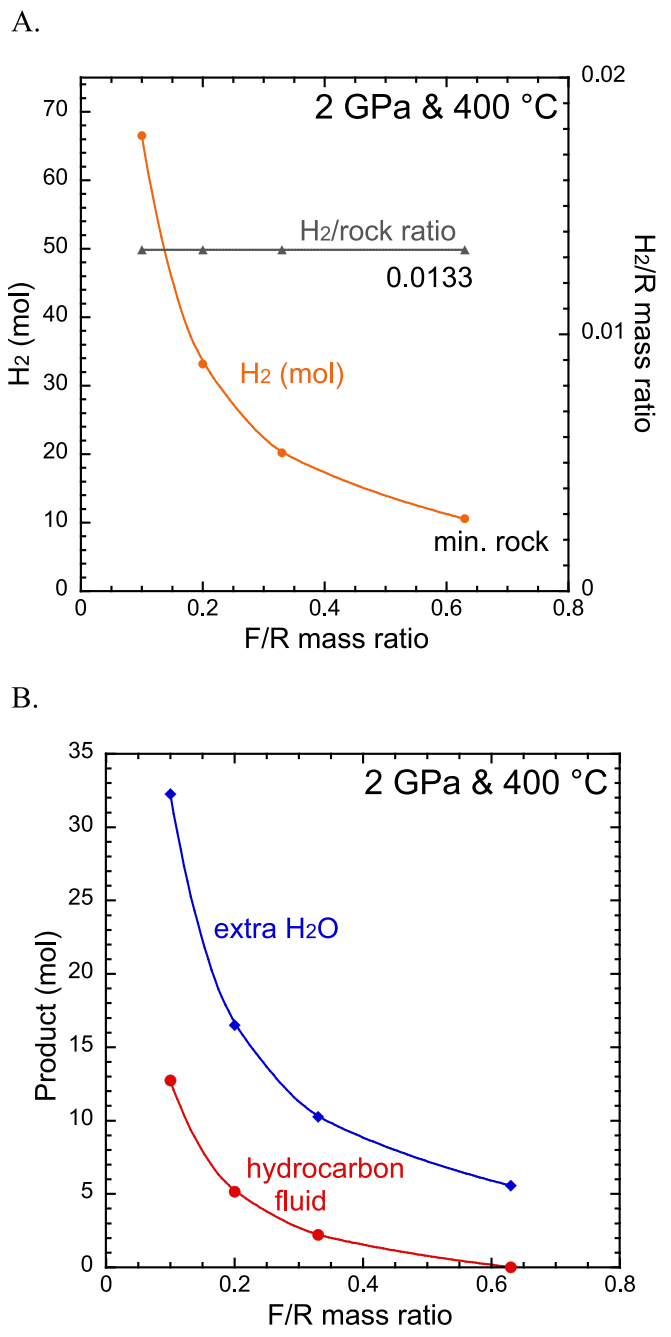

Fig. 4. (A) Number of moles of H_2 consumed and the H_2/R mass ratio vs. F/R mass ratio; (B) Number of moles of immiscible hydrocarbon fluids and excess H_2O formed vs. F/R mass ratio.

aragonite fixed f_{O_2}, total C, and methane in the fluid at constant values, until all the aragonite was destroyed.

The molality of C reached a plateau when graphite formed, and the system was buffered.

Major changes in $logf_{O_2}$ and pH can be seen in Fig. 3D. The values of $logf_{O_2}$ decreased gradually then strongly, corresponding to the continuous addition of H_2 as a function of $log\ \xi$. A plateau was reached when graphite appeared, which buffered the $logf_{O_2}$ co-existing with aragonite. After all the aragonite was destroyed, the $logf_{O_2}$ dropped quickly to the value where graphite and hydrocarbon fluids (almost pure CH_4) could co-exist. The final $logf_{O_2}$ was −30.2 (QFM−4.1). The initial pH was very alkaline with significant amounts of Ca and Mg (Table 1). Overall, it was a $Mg(OH)_2$ and $Ca(OH)_2$ solution. Interestingly, the pH became even more alkaline with $log\ \xi$ as more Ca was added to the fluid by dissolution of aragonite (Fig. 3D). The rate of increase slowed when clinopyroxene (ss) appeared, and then reached a peak after brucite appeared, resulting in buffering of the pH at 5.80. The pH decreased a little to 5.77 corresponding to the formation of the hydrocarbon fluids.

The change of concentrations of individual aqueous species mirrors the above changes in the $logf_{O_2}$, pH, and mineral products (Fig. 3E). It can be seen that $CH^0_{4,aq}$ was the most abundant aqueous C-species and increased until graphite formed after which it increased again. These changes correspond to the conversion of the carbonate in aragonite to graphite and then to methane. The trends of the other aqueous hydrocarbon species were similar. Carbonate species decreased all the way because of the drop of $logf_{O_2}$. The molality of $H^0_{2,aq}$ did not increase much until the last stage of the reaction progress where it only reached about 0.01 m, which means that almost all the reactant H_2 were consumed by incorporation into hydrocarbons as well as oxidation to H_2O and OH-groups in brucite.

4.2.2. *Models at 2.0 GPa and 400 °C with different initial F/R mass ratios*

The standard model discussed above referred to an initial F/R ratio of 0.10 by weight. In that model, the initial mass of rock was 10.0 kg and the initial fluid contained 1.0 kg H_2O (55.51 mol). We also investigated models with higher initial F/R for two reasons. First, the F/R of natural samples are variable, and we could test differences in the model results if the decarbonation reactions were extended. Second, higher F/R ratios might represent initial carbonated serpentinites with a higher porosity. Third, higher F/R ratios imply less amounts of initial aragonite relative to 1.0 kg H_2O, which in turn requires less H_2 to destroy the aragonite and facilitate the formation of hydrocarbon fluids.

Models of four additional initial F/R ratios were calculated ranging from 0.10 to 0.63 and corresponding initial amounts of reactant H_2 from 66.5 mol to 10.6 mol, respectively (Table 2 and Figs. 4A and B). The range of the initial amount of reactant H_2 was selected in order to finish the mass transfer computation before olivine(ss) formed. The mass ratios of H_2 and rock were very similar for all the runs, around 0.0133 (Table 2 and Fig. 4A). Interestingly, even with a wide range of F/R ratios, the predicted mineral sequences, solid solution compositions, hydrocarbon fluid compositions, $logf_{O_2}$, pH, trends of dissolved elements and aqueous species were all very similar to the standard run described above. However, the absolute amounts of minerals, hydrocarbon fluids, and H_2O formed all decreased with higher F/R ratios. It can be seen in Fig. 4B that the amount of H_2O formed during the reactions decreased strongly from 32.3 to 5.57 mol, resulting in lower concentrations of elements and aqueous species than in the standard run (Fig. 4B).

The formation of hydrocarbon fluids also decreased strongly with higher F/R ratios. The number of moles of hydrocarbon fluid dropped by 3 log units corresponding to the rise in F/R from 0.10 to 0.63 (Table 2, Fig. 4B). The mass of rock after reaction decreased in every run. In the standard run, the mass of rock decreased by 7.30%. The percentage of decrease was slightly greater in runs with higher F/R (8.18%). Taking into account the final amounts of H_2O, the final values of F/R could be calculated, and they were higher than the initial F/R ratio because of the significant number of moles of excess H_2O created during the mass transfer. The percentage of increase was 10% for the initial F/R ratio of 0.63, but reached 59% for the initial F/R ratio of 0.10. To conclude, lowering the F/R increased the formation of the immiscible hydrocarbon fluids significantly because of the reduction of large amounts of aragonite. Because of the extra H_2O formed, the aqueous fluids were diluted by the oxidation of H_2 fluids and $CH^0_{4,aq}$ was the only major aqueous carbon species.

4.2.3. *Models at different temperature-pressure conditions*

To investigate the roles of temperature and pressure during the formation of hydrocarbons from the reduction of carbonated serpentinite, we expanded our conceptual model at pressure and temperature con-

ditions along the metamorphic path of the Lanzo Massif (Giuntoli et al., 2020; Vitale Brovarone et al., 2017). The pressure and temperature conditions run with the mass transfer model were 1.0 GPa and 400 °C, 1.5 GPa and 400 °C, 2.0 GPa and 450 °C, and 2.0 GPa and 500 °C (Figs. 5, 6, & 7, Table S-1 to S-4) with a F/R mass ratio of 0.1. The rock reactants were the same for each run: 16.45 mol of aragonite, 3.53 mol of antigorite, 0.71 mol of magnetite, and 1.88 mol of chlorite(ss). However, the numbers of moles of H_2 needed were 68.4, 66.4, 53.9, and 76.8, respectively, depending on the reaction conditions. At 1.5 GPa and 400 °C, the amount of H_2 corresponds to the point just before olivine(ss)

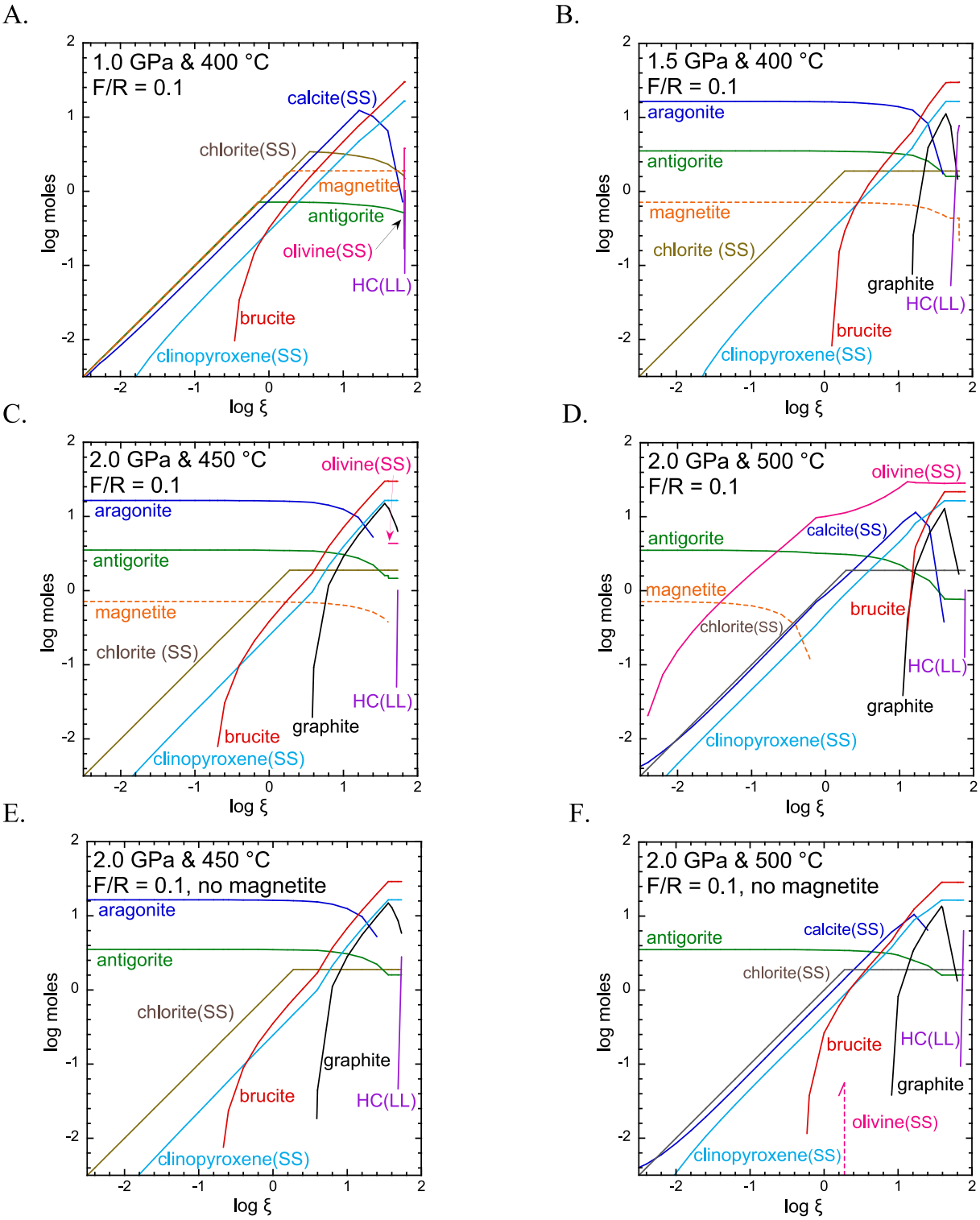

Fig. 5. Reaction path models of the destruction of carbonated serpentinites by H_2 at different temperatures and pressures with F/R equal to 0.1 (by weight). The logarithms of the number of moles of minerals produced are shown as functions of *log ξ*: (A) 1.0 GPa and 400 °C; (B) 1.5 GPa and 400 °C; (C) 2.0 GPa and 450 °C, (D) 2.0 GPa and 500 °C; and (E) 2.0 GPa and 450 °C, (F) 2.0 GPa and 500 °C GPa without initial reactant magnetite. HC(LL) refers to an immiscible fluid hydrocarbon phase. Note that all models in the figure use aragonite as the reactant carbonate mineral. In Figs. 5A, D, and F, the reactant aragonite is not plotted as it is progressively converted to calcite.

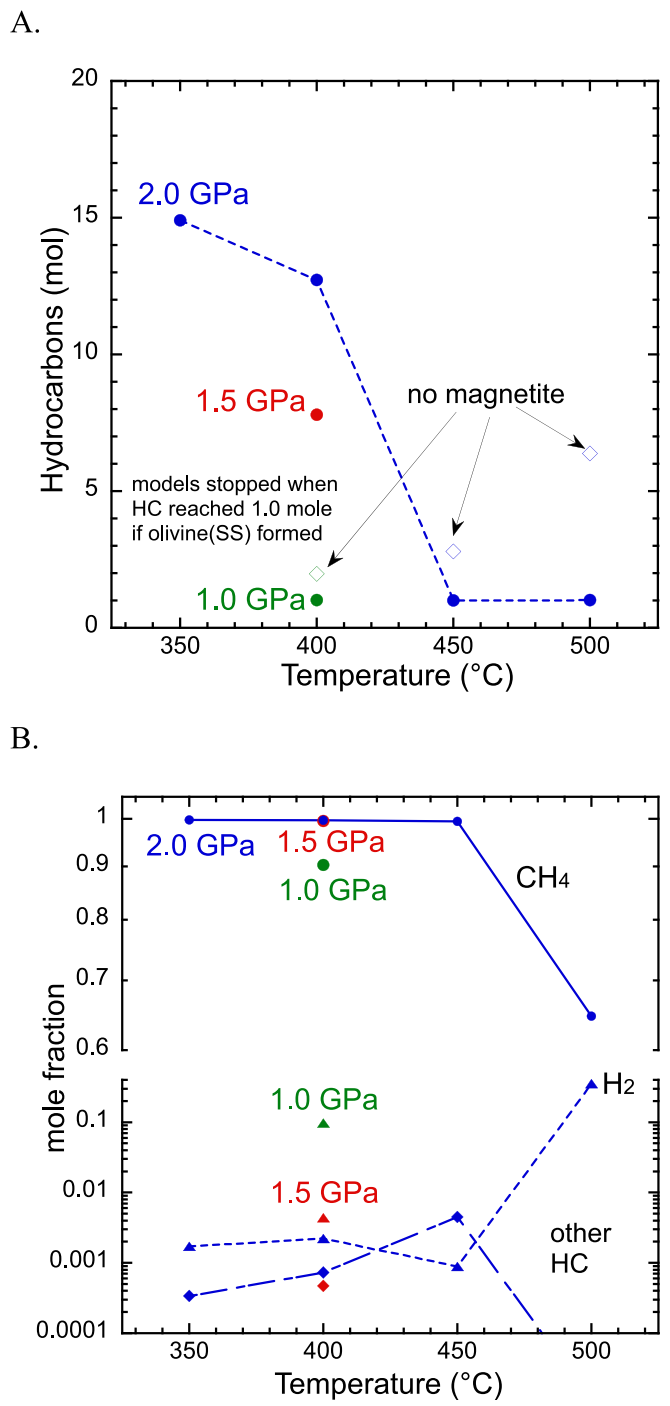

Fig. 6. (A) Number of moles of hydrocarbon fluids and (B) mole fractions of fluid hydrocarbon species vs. temperature at 1.0 (green), 1.5 (red), and 2.0 (blue) GPa. (A) Models without magnetite are represented by empty diamonds. (B) The dots and solid line represent CH_4, the triangles and dashed line represent H_2, and the diamonds and dash-dotted line represent other hydrocarbons (see text). (For interpretation of the references to colour in this figure legend, the reader is referred to the web version of this article.)

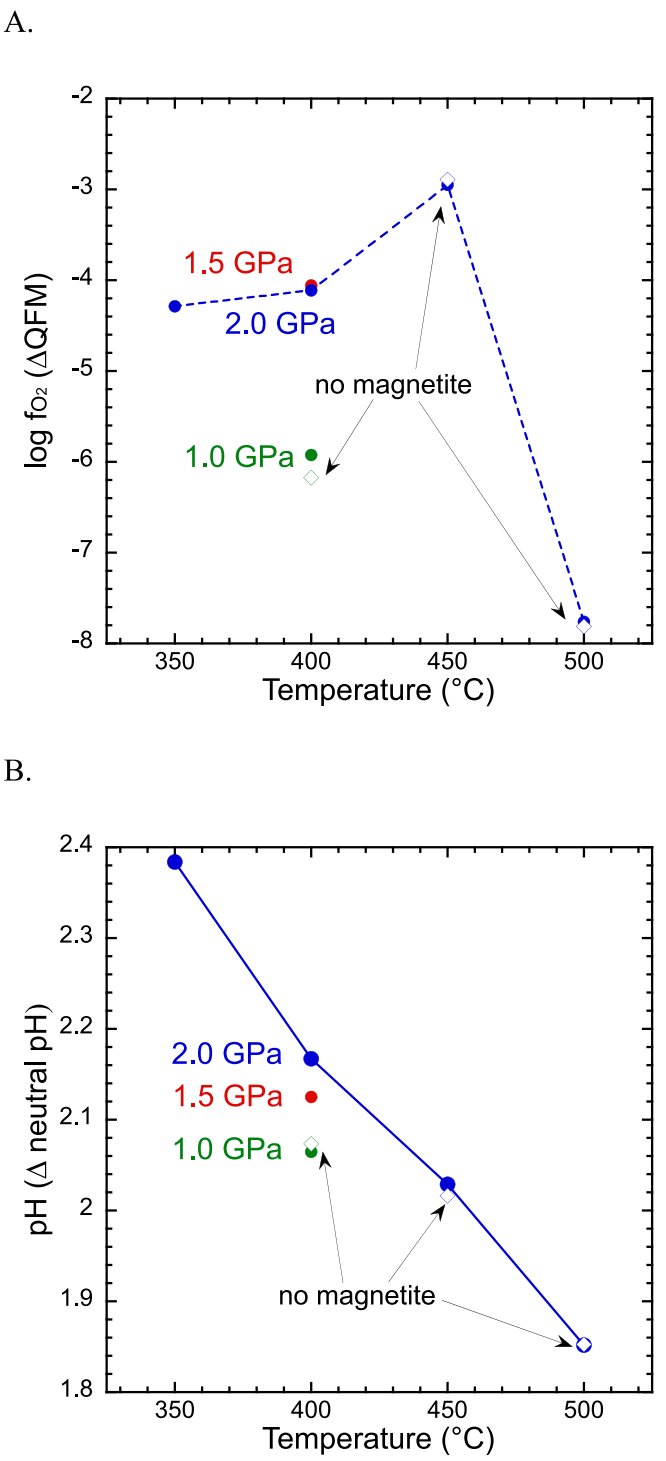

Fig. 7. (A) *Log* f_{O_2} relative to QFM and (B) *pH* relative to neutral *pH* vs. temperature at the end of the reactions with F/R 0.1 at 1.0 GPa (green), 1.5 GPa (red), and 2.0 GPa (blue). Models without magnetite are represented by empty diamonds. (For interpretation of the references to colour in this figure legend, the reader is referred to the web version of this article.)

formation, the same as the standard run at 2.0 GPa and 400 °C. However, at 1.0 GPa and 400 °C, 2.0 GPa and 450 °C, and 2.0 GPa and 500 °C, the number of moles of H_2 corresponds to the point when 1.0 mol of hydrocarbon fluids formed because olivine(ss) formed before hydrocarbon fluids.

The lowest pressure considered, 1.0 GPa and 400 °C, was on the exhumation path; other conditions were on the prograde path of the Lanzo massif (Vitale Brovarone et al., 2017). Fig. 5 presents the amounts of minerals, both reactants and products, as a function of *log* ξ. Antigorite was stable in the beginning and then decreased at all conditions. Corresponding to the molecular formula assumed for antigorite, the volume of antigorite destroyed reached about 1800 cm^3 (37% of the total volume in the system). Clinopyroxene(ss) was the first product mineral with almost pure diopside and then brucite formed in all the

runs. Chlorite(ss) with >95 mol% clinochlore did not react and stayed until the end of the runs, except for a slight decrease at 1.0 GPa and 400 °C. Hydrocarbon fluids formed during a late interval of reaction progress and increased quickly.

At 1.0 GPa and 400 °C, calcite(ss) was more stable than aragonite (Fig. 5A, Table S-1). Interestingly, this, the retrograde path model, was the only model without graphite formation. Hydrocarbon fluids formed directly from calcite(ss). As mentioned above, graphite is not stable relative to aragonite for certain levels of the ratio $a_{Ca^{2+}}/a^2_{H^+}$ in the aqueous phase. At this pressure and temperature, graphite cannot be stable when the aqueous fluid has a $log\left(a_{Ca^{2+}}/a^2_{H^+}\right)$ value <9.50. In the run shown in Fig. 5A, the value of $log\left(a_{Ca^{2+}}/a^2_{H^+}\right)$ changed from an initial value of 9.29 to a final value of 9.46. Fe-rich olivine(ss) with $X_{Fayalite}$ 0.29 formed near the endpoint and increased rapidly to 3.8 mol before hydrocarbons appeared.

The model at 1.5 GPa and 400 °C (Fig. 5B, Table S-2) was similar to the standard model at 2.0 GPa and 400 °C in terms of the mineral sequence, the relative amounts of minerals, and the amount of H_2 reactant. However, the model at 2.0 GPa and 450 °C (Fig. 5C, Table S-3) showed the same mineral sequence as the standard model until magnetite was totally consumed and then olivine(ss) formed before the formation of hydrocarbon fluids. The olivine was Fe-rich ($X_{Fayalite}$ 0.26), representing a metasomatic composition. It appeared that the breakdown of magnetite caused by the addition of H_2 provided Fe^{2+} that stabilized olivine. If more H_2 was added, olivine became unstable and was reduced to metallic iron. The amount of H_2 (53.9 mol) used here represents the value when 1.0 mol of hydrocarbon formed co-existing with graphite. Graphite was completely destroyed for values of H_2 equal to or >66.5 mol.

Interestingly, our model at 2.0 GPa and 500 °C (Fig. 5D, Table S-4) contained olivine with antigorite throughout the reaction progress. As magnetite started to decrease sooner in this model, the formation of olivine(ss) was even more strongly favored, and it became the most abundant mineral quickly. When magnetite was destroyed, the iron content of the olivine reached a peak at Fa 21, but then the rate of olivine increase slowed. Forsterite started to increase and finally reached the upper mantle composition (Fo 93). If more H_2 was added, even up to 90.0 mol, no metallic iron formed and the hydrocarbon fluids ended up very H_2-rich. Calcite(ss) was more favored than aragonite at this condition and was reduced to form graphite and then hydrocarbon fluids. Graphite formed only slightly before brucite.

In order to investigate the effect of magnetite destruction on the formation of olivine(ss), we tested models without magnetite as a reactant. At 2.0 GPa and 450 °C, without reactant magnetite in the initial rock, we found that only a very small amount of magnetite formed and then disappeared during the run. The log number of moles of magnetite was −5.7 to −5.0 during $log\ \xi$ from −3.8 to −2.6. This small amount of magnetite simply reflected the (low) amount of Fe in the initial fluid. No olivine formed. However, for the model at 2.0 GPa and 500 °C also without magnetite, a very small and transient amount of olivine(ss) appeared (Fig. 5F), but at a much later stage of reaction progress than in Fig. 5D at the same pressure and temperature. Only 0.056 mol of olivine(ss) formed from $log\ \xi$ at 0.20–0.28 and then disappeared. No extra olivine(ss) formed even if more H_2 was added. The excess H_2 stayed in the hydrocarbon fluids at 2.0 GPa and 500 °C and the hydrocarbon fluids became H_2-rich.

To summarize, if magnetite was present as a reactant in our models, olivine would form. If reactant magnetite was not included in our models, olivine(ss) formation would not form at both 450 and 500 °C. We note that in the natural samples, although magnetite is often present, no preserved olivine was observed. The reason for this discrepancy may lie in the highly heterogeneous nature of the Lanzo carbonated serpentinite or be due to retrograde hydration. If H_2 fluid pathways did not encounter magnetite, or the amount of magnetite encountered was very low, our models indicate that olivine would not be expected to form to a significant extent. We also note that in other natural samples involving high temperature and high pressure and serpentinite breakdown, epitaxial growth of magnetite in olivine-hosted fluid inclusions can occur (Campione et al., 2020; Malaspina et al., 2023). Such systems may represent very different oxidation states to the very reducing ones in our models.

Hydrocarbon fluids formed at the end of the reactions at each pressure and temperature condition are presented in Figs. 5A - F. The final amounts and compositions of the hydrocarbon fluids can be seen in Fig. 6 over the range of 1.0–2.0 GPa and 350–500 °C. At the higher pressures and lower temperatures, if olivine(ss) did not form, hydrocarbon fluid formation was favored (Fig. 6A). The reason is simply that the saturation activity of $CH_{4,aq}$ was smaller at higher pressure and lower temperature. In models without magnetite, more hydrocarbons formed, and the degree of increase is greater at higher temperature. Except for the models at 2.0 GPa, 450 °C and 500 °C, the amounts of H_2 were about 66.0 mol. If the saturation activity of $CH^0_{4,aq}$ were smaller (i.e. the solubility was lower), more $CH_{4,f}$ could equilibrate in hydrocarbons.

The fluid compositions shown in Fig. 6B indicate that $CH_{4,f}$ was the most abundant endmember of the immiscible fluids over the temperature range considered. Except at 2.0 GPa and 500 °C, the hydrocarbon was almost pure $CH_{4,f}$ with a mole fraction larger than 0.90. At 2.0 GPa, from 450 °C to 500 °C, the mole fraction of $CH_{4,f}$ dropped from 0.99 to 0.65 as the $H_{2,f}$ component increased up to 0.35. However, other hydrocarbons were negligible. At 1.0 GPa, the mole fraction of $H_{2,f}$ was much greater than at higher pressures at 400 °C. No significant effect on the composition of fluids by pressure was observed. Overall, the fluids were methane-rich without olivine. If more initial H_2 were added, the curves would move towards more H_2-rich compositions. After all the carbon was reduced by the reactant H_2, the $H_{2,f}$ became unreactive and built up as a component in the hydrocarbon fluid.

The final $logf_{O_2}$ at each condition with an F/R equal to 0.1 is given relative to the QFM buffer in Fig. 7A. The highest $logf_{O_2}$ was at 2.0 GPa and 450 °C because hydrocarbon fluids formed coexisting with graphite with the lowest initial number of H_2 moles. The $logf_{O_2}$ at 400 °C of both 1.5 and 2.0 GPa were very close, as were the other results for minerals, aqueous species, and hydrocarbon compositions at these conditions. At 2.0 GPa and 350 °C, the $logf_{O_2}$ was lower probably because olivine(ss) was not favored at low temperature and only formed at temperatures >400 °C. The models at 500 °C had the largest initial number of H_2 moles. This large amount of H_2 resulted in the total reduction of oxidized C and the excess H_2 caused extremely reducing conditions (Fig. 7A). The final $logf_{O_2}$ values of the models were not affected significantly by removing magnetite as a reactant.

The final pH value of each model (relative to neutral pH) with F/R equal to 0.1 is plotted in Fig. 7B. It can be seen that the final ΔpH values increased <0.2 compared to the initial pH values. The fluids are basically $Mg-Ca-OH$ fluids. All of the fluids were alkaline because brucite was in equilibrium with the aqueous fluids, and contributed to Mg^{2+} and OH^-. At 2.0 GPa, the final pH decreased with temperature resulting in less alkaline aqueous fluids. The final Ca concentrations were observed decreasing from 0.038 to 0.021 m with temperature at 2.0 GPa (Table S1–4). Lower Ca concentrations resulted in lower values of the pH. At 400 °C, the final pH increased from 1.0 to 2.0 GPa. The opposite trend of Ca concentration showed that Ca increased from 0.008 to 0.031 m with pressure at 400 °C. Interestingly, the drop of pH was affected more by temperature even when Ca decreased by 0.017 m. Again, the final pH values of the models were not affected by removing magnetite from the reactants.

Overall, the above models demonstrated that hydrocarbons could form over a wide range of pressure and temperature conditions, during both the prograde metamorphism and exhumation processes of the Lanzo Massif (Vitale Brovarone et al., 2017). The process of hydrocarbon formation was systematically the same as the standard model within the pressure range of 1.5 to 2.0 GPa and a temperature range of 400 to

450 °C. The product minerals diopside, brucite, and graphite were consistent with the natural samples at 1.5 to 2.0 GPa. Our model with expanded pressure and temperature conditions predicted small variations of mineral assemblages and hydrocarbon compositions.

4.2.4. Garnet formation

The model results presented above could reproduce with a good confidence level the natural features described by Vitale Brovarone et al. (2017). However, in other samples from the same locality, Giuntoli et al. (2020) also reported the presence of Ca-Fe-rich garnet forming along carbonate reduction channels. The formation of Ca-Fe-rich garnet was not predicted by our models for low carbonate/serpentinite ratios (15 vol% aragonite; 85 vol% serpentinite) at 2.0 GPa and 400 °C provided that we chose an appropriate standard Gibbs free energy of andradite less stable than that reported by Moecher and Chou (1990). However, using the same characterization of andradite, Ca-Fe-rich garnet did form at 2.0 GPa and 400 °C when we performed complementary models for two higher carbonate/serpentinite ratios (30 vol% aragonite, 70 vol% serpentinite; and 50 vol% aragonite, 50 vol% serpentinite) consistent with the results described by Giuntoli et al. (2020). In these latter two models, the final mineral assemblage, after antigorite and chlorite were exhausted, brucite, clinopyroxene, aragonite, graphite, and Ca-rich-garnet together with hydrocarbon fluid (see Appendix A).

5. Discussion

We have carried out the first chemical mass transfer models of water-rock interaction involving the prediction of immiscibility of the aqueous phase fluid hydrocarbon or H_2-rich phases. The calculations were possible because we were able to use a mass transfer code in a novel way (section 3.3, above). The results of the simulations described above are therefore novel. The credibility of the present results rests on a comparison with the detailed published studies of the alteration of the Lanzo carbonated serpentinites. We discuss the comparison next and also discuss more general implications.

5.1. Comparison of model results with the altered Lanzo carbonated serpentinites

Our study has established predictive models of the formation of immiscible hydrocarbon fluid during the reaction of H_2 with carbonated serpentinite at temperatures and pressures relevant to subduction zones. Here we compare the model results with the previously reported petrographic results in Vitale Brovarone et al. (2017). As summarized above in Section 2, the overall reaction suggested for the carbonated serpentinite reduction and hydrocarbon formation as in Eq. (1) indicates that antigorite and Ca-carbonate reacted with H_2 to form clinopyroxene, brucite, methane, and water. The results for our standard model (Fig. 3) agree with this generalized reaction. However, the generalized reaction does not capture all the petrographic detail. For example, the generalized reaction does not include graphite specifically. In contrast, the detailed petrography indicates the stepwise formation of methane involving graphite as described next.

The natural samples contain evidence that Ca-carbonate was first reduced to methane and graphite and then graphite was altered to methane during protracted H_2 infiltration (Vitale Brovarone et al., 2017). A recent experimental study is consistent with the proposed latter process (Peña-Alvarez et al., 2021). An overall reaction for alteration of Ca-carbonate to graphite was already given in Eqs. (7) and (8). Here we present more detail. In most of our models, Ca-carbonate was first reduced to $CH_{4,aq}$ by H_2, which can be expressed as

$$CaCO_3 + 4H_{2,f} = Ca(OH)^+ + OH^- + CH_{4,aq} + H_2O \quad (10)$$

This reaction contributes to the early increases in pH and $CH^0_{4,aq}$ seen in Figs. 3D and E. The $logf_{O_2}$ continued to decrease and $a_{CH_{4,aq}}$ increased to reach the equilibrium between $CH^0_{4,aq}$ and graphite, coexisting with the reactant Ca-carbonate, which can be expressed by

$$CH^0_{4,aq} + CaCO_3 = 2C^{graphite} + Ca(OH)^+ + OH^- + H_2O \quad (11)$$

During the co-existence of aragonite and graphite, $logf_{O_2}$ was buffered (Fig. 3D). But with even more H_2 reacting, eventually the aragonite was completely destroyed and the $logf_{O_2}$ dropped associated with an increase in the $a_{CH^0_{4,aq}}$. In turn, these changes destabilized graphite in favor of CH_4-rich fluid according to Eq. (9) above. In this way, the model predicted the formation of graphite from aragonite, and subsequently the formation of immiscible hydrocarbon fluid from graphite. The model prediction is therefore in agreement with the data for the natural samples with regard to an important sequence of events.

Another way to compare the model results with the natural samples is to examine the fluid chemistry. The fluid inclusions reported for the altered carbonated serpentinite (Section 2) were mostly $CH_4 - H_2$-rich (plus minor ethane), associated with graphite rims on serpentinite clasts. Minor amounts of H_2O-bearing inclusions were related to graphite-free serpentinite clasts. The first type is approximated by our model immiscible hydrocarbon fluid. At 2.0 GPa and 400 °C, the model fluid is predominantly CH_4 with minor H_2 and very minor amounts of ethane as the second most abundant hydrocarbon. Despite the approximations in our model regarding ideal solution in the hydrocarbon fluid, the above results are reasonably consistent with the actual fluid inclusions. The H_2O-bearing fluid inclusions associated with graphite-free partially reacted carbonated serpentinites, could represent an early stage in our models with higher $logf_{O_2}$ and lower $a_{CH^0_{4,aq}}$.

5.2. Carbon and Hydrogen budget during hydrocarbon formation

In all our models, the carbon in the initial system is almost entirely present in the carbonated serpentinites as a carbonate mineral. In the standard model at 2.0 GPa and 400 °C, when hydrocarbon fluid first appeared at $log\ \xi$ of 1.61, the carbon budget in moles was 76.5%, 0.2%, and 23.3% of graphite, hydrocarbon, and aqueous carbon, respectively. Graphite then dropped to only 9.3%, whereas hydrocarbons increased to 67.5%, and aqueous carbon remained about the same. In the final step, the hydrocarbon fluid contained 77.1% and aqueous carbon contained 22.9% of the total carbon.

The budget of hydrogen (H) is also important because H from the influx of $H_{2,f}$ can be incorporated into antigorite and brucite, as well as aqueous and hydrocarbon fluids. The H in the initial system before $H_{2,f}$ reacted was almost all in antigorite and the initial water. The mole percentages were 49.6% and 50.4%, respectively.

However, the final hydrogen budget (Table 3) shows that H_2O still took up nearly half of the H even after 66.5 mol of $H_{2,f}$ were added to the system. A lot of H_2O formed during the reactions and brucite was the second most abundant species containing 17.7% of the total H. Antigorite contained only 14.1%. Methane in the hydrocarbon fluid constituted 14.4% of the total hydrogen, but $CH_{4,aq}$ constituted only 4.2% of the total hydrogen. Compared with the carbon budget, the hydrogen budget was more complex because multiple types of H-bearing species existed in models at all temperature-pressure conditions, and were not affected by the carbon mineral sequences, although the percentages varied. Overall, both the carbon and hydrogen budgets were useful tools for tracking the redox reactions systematically.

Table 3
The final hydrogen budget (mole of element percentage) of the model at 2.0 GPa & 400 °C with $\boldsymbol{F/R}$ 0.1.

Mineral		Aqueous fluid		Hydrocarbon fluid	
antigorite	antigorite	$CH_{4,aq}$	4.2%	$CH_{4,f}$	14.4%
brucite	17.7%	H_2O	49.6%		
chlorite	<1%	$Mg(OH)_2$	<1%		

5.3. Origin of H_2 fluids that reacted with carbonated serpentinites in the Lanzo Massif

The origin of the large amounts of H_2 fluid involved in the alteration of the Lanzo carbonated serpentinties is an interesting topic. It has been suggested that the H_2 could have originated by serpentinization of the fresh peridotite rocks in the massif during subduction and then migrated along channelized fluid pathways (Debret et al., 2013; Vitale Brovarone et al., 2017, 2020). Typically, H_2 can be generated by the oxidation of the fayalite endmember in primary peridotitic olivine, which can be expressed as

$$3Fe_2SiO_4 + 2H_2O \rightarrow 2Fe_3O_4 + 3SiO_{2,aq} + 2H_2 \quad (12)$$

The above reaction enables an estimate of the amount of olivine that would need to be serpentinized to provide all the H_2 for making CH_4. For example, at 2.0 GPa and 400 °C, 66.5 mol of $H_{2,f}$ were needed to form 12.7 mol of $CH_{4,f}$. According to Eq. (12), 99.75 mol of fayalite would be needed. If we assume that the mole fraction of fayalite in the peridotitic olivine was 7%, then 1325 mol of forsterite should be serpentinized. Using the following serpentinization reaction

$$34Mg_2SiO_4 + 51H_2O \rightarrow Mg_{48}Si_{34}O_{85}(OH)_{62} + 20Mg(OH)_2 \quad (13)$$

the 1325 mol of forsterite should produce 39 mol of antigorite. Overall, to form 66.5 mol of $H_{2,f}$ (around 903 cm^3) and 12.7 mol of $CH_{4,f}$, about 0.06 m^3 of olivine were destroyed and about 0.07 m^3 of antigorite were created. These quantities of minerals are small compared to the amounts available in a massif.

$CH_4 - H_2$-rich fluid inclusions have also been found in the high-pressure serpentinized ultramafic peridotites of other subduction zone complexes (Boutier et al., 2021; Vitale Brovarone et al., 2020). Additional reduced fluid species such as H_2S and NH_3 were found in some of the preserved inclusions. The condition of high-pressure serpentinization happened near the peak metamorphic condition, 370–400 °C and 1 GPa for the eclogitic-facies Lanzo massif. Graphitic carbon was not commonly observed, which is consistent with our model at those temperature and pressure conditions (Fig. 5A; see section 4.2.3). The $log\, f_{O_2}$ of serpentinization was inferred to be less than QFM because awaruite was associated with antigorite. CH_4 in the fluid inclusions was thought to have been formed by reduction of carbon in the serpentinizing fluid.

6. Conclusions

We have focused on predicting the formation of immiscible hydrocarbon fluids at upper mantle conditions. We set up initial aqueous speciation and solubility models in equilibrium with carbonated serpentinite consistent with the natural samples reported by Vitale Brovarone et al. (2017) and Giuntoli et al. (2020). The initial fluids were then used in chemical mass transfer models simulating the irreversible reactions during the reduction of carbonated serpentinites by invading H_2 fluids. Immiscible hydrocarbon fluids formed in association with major changes of mineralogy and aqueous solution chemistry. The models covered a pressure-temperature range of 1.0–2.0 GPa and 350–500 °C.

We found the following principal results from this modeling study:

- Chemical mass transfer models predicted minerals and hydrocarbon fluids consistent with field and laboratory observations in Vitale Brovarone et al. (2017) and Giuntoli et al. (2020):
  a) Serpentinite (antigorite, magnetite, and chlorite) and aragonite were destroyed.
  b) Brucite, clinopyroxene(ss), graphite, and immiscible hydrocarbon fluids (and sometimes olivine(SS)) were formed at 1.5 and 2.0 GPa and 400–500 °C.
  c) For high initial carbonate/serpentinite ratios, Ca-Fe-rich garnet was formed at 400 °C and 2.0 GPa.
  d) Methane was the main constituent of the immiscible hydrocarbon fluids and also reached m concentrations in the coexisting aqueous fluids.
- As an example, the reaction progress during our standard run at 2.0 GPa and 400 °C with F/R mass ratio of 0.10 revealed the sequence of mineral formation, the number of moles and volumes of each mineral, the aqueous fluid composition and speciation, and the evolution of the $logf_{O_2}$ and pH. During the reactions, aragonite was reduced by H_2 to form graphite and then graphite was reduced to hydrocarbon fluid (almost pure $CH_{4,f}$) associated with an almost continuous drop of $logf_{O_2}$.
- The reaction of H_2 with carbonated serpentinite generated significant amounts of H_2O.
- Lower F/R (aqueous fluid/rock) ratios imply more H_2 fluids, which resulted in greater amounts of H_2O and hydrocarbon fluids formed.
- At 1.0 GPa and 400 °C, graphite was not stable due to the $log\left(a_{Ca^{2+}}/a^2_{H^+}\right)$ of the system being too low.
- Even small amounts of magnetite in the initial rock caused olivine(ss) to appear before hydrocarbon formation in models at 1.0 GPa and 400 °C, 2.0 GPa and 450 °C, and 2.0 GPa and 500 °C. Olivine was not stable if the reactant carbonated serpentinite did not contain magnetite.
- Carbon and hydrogen budgets trace the transfer and redistribution of these elements during the redox reactions.
- Overall, the combined results of the modeling study and the natural samples strongly support the concept that CH_4-rich immiscible hydrocarbon fluids have formed at eclogite facies conditions in subduction zones. How widespread this phenomenon is (at the present and in the geologic past) remains to be seen.

Declaration of competing interest

The authors declare that they have no known competing financial interests or personal relationships that could have appeared to influence the work reported in this paper.

Data availability

The files of the model results are available on Johns Hopkins Research Data Repository using the DOI given below. The data can be referred to using the citation below.

Huang, Jingyi; Sverjensky, Dimitri A.; Daniel, Isabelle; Brovarone, Alberto Vitale, 2022, "Data associated with: Reaction path model of the formation of abiotic immiscible hydrocarbon fluids in subducted carbonated serpentinites, Lanzo Massif (Western Italian Alps)", https://doi.org/10.7281/T1/NLHSKE, *Johns Hopkins Research Data Repository*.

Acknowledgements

This material is based upon work supported by the U.S. Department of Energy, Office of Science, Basic Energy Sciences, Geosciences program under Award Number DE-SC0019830 as well as NSF Petrology and Geochemistry Grant Number 2032039, and a Johns Hopkins Graduate Fellowship. This work is also part of a project that has received funding from the European Research Council (ERC) under the European Union's Horizon 2020 research and innovation programme (Grant agreement No. 864045). This work also received support by the Richard Lounsbery foundation. We would like to thank Daniel Viete for reading a version of this manuscript. We gratefully acknowledge the help and support of the Johns Hopkins University. We thank Fang Huang and Zhigang Zhang for discussions.

Appendix A. Supplementary data

The supplementary material contains the description of model files and tables about the summary of the initial and final fluid compositions and mineral assemblages. The files contain model results of H_2 fluid reacting with carbonated serpentinites with 15 vol% of aragonite and 85 vol% of serpentinite at 2.0 GPa and 400 °C, 1.0 GPa and 400 °C, 1.5 GPa and 400 °C, 2.0 GPa and 450 °C, and 2.0 GPa and 500 °C; with 30 vol% of aragonite and 70 vol% of serpentinite at 400 °C and 2.0 GPa; and with 50 vol% of aragonite and 50 vol% of serpentinite at 400 °C and 2.0 GPa. Supplementary data to this article can be found online at https://doi.org/10.1016/j.lithos.2024.107498.

References

Alt, J.C., Schwarzenbach, E.M., Früh-Green, G.L., Shanks, W.C., Bernasconi, S.M., Garrido, C.J., Crispini, L., Gaggero, L., Padrón-Navarta, J.A., Marchesi, C., 2013. The role of serpentinites in cycling of carbon and sulfur: Seafloor serpentinization and subduction metamorphism. Lithos 178, 40–54.

Barbier, S., Huang, F., Andreani, M., Tao, R., Hao, J., Eleish, A., Prabhu, A., Minhas, O., Fontaine, K., Fox, P., Daniel, I., 2020. A Review of H2, CH4, and Hydrocarbon Formation in Experimental Serpentinization using Network Analysis. Front. Earth Sci. 8 (June), 1–20.

Berman, R.G., 1988. Internally-Consistent Thermodynamic Data for Minerals in the System Na2O-K2O-CaO-MgO-FeO-Fe2O3-Al2O3-SiO2-TiO2-H2O-CO2. J. Petrol. 29 (2), 445–522.

Boutier, A., Vitale Brovarone, A., Martinez, I., Sissmann, O., Mana, S., 2021. High-pressure serpentinization and abiotic methane formation in metaperidotite from the Appalachian subduction, northern Vermont. Lithos 396–397, 106190.

Boutier, A., Martinez, I., Sissmann, O., Agostini, S., Daniel, I., Van Baalen, M., Mana, S., Vitale Brovarone, A., 2023. Complexity of graphite formation in response to metamorphic methane generation and transformation in an orogenic ultramafic body. Geochim. Cosmochim. Acta 364, 166–183.

Campione, M., La Fortezza, M., Alvaro, M., Scambelluri, M., Malaspina, N., 2020. Commensurate growth of Magnetite Microinclusions in Olivine under Mantle Conditions. ACS Earth Space Chem. 4 (6), 825–830.

Dasgupta, R., Hirschmann, M.M., 2010. The deep carbon cycle and melting in Earth's interior. Earth Planet. Sci. Lett. 298, 1–13.

Debret, B., Nicollet, C., Andreani, M., Schwartz, S., Godard, M., 2013. Three steps of serpentinization in an eclogitized oceanic serpentinization front (Lanzo Massif - Western Alps). J. Metamorph. Geol. 31 (2), 165–186.

Foustoukos, D.I., Stern, J.C., 2012. Oxidation pathways for formic acid under low temperature hydrothermal conditions: Implications for the chemical and isotopic evolution of organics on Mars. Geochim. Cosmochim. Acta 76, 14–28.

Giuntoli, F., Vitale Brovarone, A., Menegon, L., 2020. Feedback between high-pressure genesis of abiotic methane and strain localization in subducted carbonate rocks. Sci. Rep. 10 (1), 1–15.

Gold, T., 1992. The deep, hot biosphere. Proc. Natl. Acad. Sci. U. S. A. 89 (13), 6045–6049.

Gold, T., 2001. The Deep Hot Biosphere: The Myth of Fossil Fuels. Springer Science & Business Media.

Hacker, B.R., Abers, G.A., Peacock, S.M., 2003. Subduction factory 1. Theoretical mineralogy, densities, seismic wave speeds, and H 2 O contents. J. Geophys. Res. Solid Earth 108 (B1).

Holt, A.F., Condit, C.B., 2021. Slab temperature evolution over the lifetime of a subduction zone. Geochem. Geophys. Geosyst. 22 (6).

Huang, F., Sverjensky, D.A., 2019. Extended deep earth water model for predicting major element mantle metasomatism. Geochim. Cosmochim. Acta 254, 192–230.

Huang, F., Daniel, I., Cardon, H., Montagnac, G., Sverjensky, Di.A., 2017. Immiscible hydrocarbon fluids in the deep carbon cycle. Nat. Commun. 8 (May).

Huang, J., Daniel, I., Sverjensky, D.A., Cardon, H., Montagnac, G., 2023. Formation of hydrocarbons favored by high pressure at subduction zone conditions. Chem. Geol. 630, 121489.

Klein, F., Grozeva, N.G., Seewald, J.S., 2019. Abiotic methane synthesis and serpentinization in olivine-hosted fluid inclusions. Proc. Natl. Acad. Sci. U. S. A. 116 (36), 17666–17672.

Kolesnikov, A., Kutcherov, V.G., Goncharov, A.F., 2009. Methane-derived hydrocarbons produced under upper-mantle conditions. Nat. Geosci. 2 (8), 566–570.

Kolesnikov, A.Y., Saul, J.M., Kutcherov, V.G., 2017. Chemistry of Hydrocarbons under Extreme Thermobaric Conditions. ChemistrySelect 2 (4), 1336–1352.

Kudryavtsev, N., 1951. Against the organic hypothesis of the origin of petroleum. Neftianoye Khozyaistvo 9, 17–29.

Kudryavtsev, N.A., 1959. Geological proof of the deep origin of petroleum. *Trudy Vsesoyuz*. Neftyan. Nauch. Issledovatel Geologoraz Vedoch. Inst. 132, 242–262.

Kutcherov, V.G., Krayushkin, V.A., 2010. Deep-seated abiogenic origin of petroleum: from geological assessment to physical theory. Rev. Geophys. 48 (1), 1–30.

Lagabrielle, Y., Fudral, S., Kienast, J.-R., 1990. La couverture océanique des ultrabasites de Lanzo (Alpes occidentales): arguments lithostratigraphiques et pétrologiques. Geodin. Acta 4 (1), 43–55.

Li, Y., 2017. Immiscible CHO fluids formed at subduction zone conditions. Geochem. Pespect. Lett. 3, 12–21.

Malaspina, N., Campione, M., Tumiati, S., Murri, M., Fumagalli, P., Cerantola, V., La Fortezza, M., Scambelluri, M., 2023. Epitactic magnetite growth in fluid inclusions as driving force for olivine oxidation coupled with hydrogen production at high pressure. Chem. Geol. 629.

Manning, C.E., Shock, E.L., Sverjensky, D.A., 2013. The chemistry of carbon in aqueous fluids at crustal and upper-mantle conditions: Experimental and theoretical constraints. Rev. Mineral. Geochem. 75, 109–148.

McCollom, T.M., 2013. Laboratory simulations of abiotic hydrocarbon formation in earth's deep subsurface. Rev. Mineral. Geochem. 75, 467–494.

McDermott, J.M., Seewald, J.S., German, C.R., Sylva, S.P., 2015. Pathways for abiotic organic synthesis at submarine hydrothermal fields. Proc. Natl. Acad. Sci. U. S. A. 112 (25), 7668–7672.

Mendeleev, D., 1877. L'origine du petrole. Rev. Sci. 2e Ser. (VIII), 409–416.

Moecher, D.P., Chou, I.-M., 1990. Experimental investigation of andradite and hedenbergite equilibria employing the hydrogen sensor technique, with revised estimates of Delta Gf 0 (sub m,298) for andradite and hedenbergite. Am. Mineral. 75 (11–12), 1327–1341.

Mukhina, E., Kolesnikov, A., Kutcherov, V., 2017. The lower pT limit of deep hydrocarbon synthesis by CaCO3 aqueous reduction. Sci. Rep. 7 (1).

Pelletier, L., Müntener, O., 2006. High-pressure metamorphism of the Lanzo peridotite and its oceanic cover, and some consequences for the Sesia-Lanzo zone (northwestern Italian Alps). Lithos 90 (1–2), 111–130.

Peña-Alvarez, M., Brovarone, A.V., Donnelly, M.E., Wang, M., Dalladay-Simpson, P., Howie, R., Gregoryanz, E., 2021. In-situ abiogenic methane synthesis from diamond and graphite under geologically relevant conditions. Nat. Commun. 12 (1).

Penniston-Dorland, S.C., Kohn, M.J., Manning, C.E., 2015. The global range of subduction zone thermal structures from exhumed blueschists and eclogites: Rocks are hotter than models. Earth Planet. Sci. Lett. 428, 243–254.

Piccoli, F., Rubatto, D., Ovtcharova, M., Hermann, J., Guillong, M., Vitale Brovarone, A., 2023. Dating fluid infiltration and deformation in the subducted ultramafic oceanic lithosphere by perovskite geochronology. Chem. Geol. 615.

Proskurowski, G., Lilley, M.D., Seewald, J.S., Früh-Green, G.L., Olson, E.J., Lupton, J.E., Sylva, S.P., Kelley, D.S., 2008. Abiogenic hydrocarbon production at lost city hydrothermal field. Science 319 (5863), 604–607.

Pruteanu, C.G., Ackland, G.J., Poon, W.C.K., Loveday, J.S., 2017. When immiscible becomes miscible—methane in water at high pressures. Sci. Adv. 3 (8), e1700240.

Reeves, E.P., Fiebig, J., 2020. Abiotic synthesis of methane and organic compounds in earth's lithosphere. Elements 16 (1), 25–31.

Rubatto, D., Hermann, J., 2001. Exhumation as fast as subduction? Geology 29 (1), 3–6.

Scambelluri, M., Cannaò, E., Gilio, M., 2019. The water and fluid-mobile element cycles during serpentinite subduction. A review. Eur. J. Mineral. 31 (3), 405–428.

Sephton, M.A., Hazen, R.M., 2013. On the origins of deep hydrocarbons. Rev. Mineral. Geochem. 75, 449–465.

Sverjensky, D.A., 2019. Thermodynamic modelling of fluids from surficial to mantle conditions. J. Geol. Soc. Lond. 176 (2), 348–374.

Sverjensky, D.A., Hemley, J.J., D'angelo, W.M., 1991. Thermodynamic assessment of hydrothermal alkali feldspar-mica-aluminosilicate equilibria. Geochim. Cosmochim. Acta 55 (4), 989–1004.

Sverjensky, D.A., Harrison, B., Azzolini, D., 2014. Water in the deep Earth: the dielectric constant and the solubilities of quartz and corundum to 60kb and 1200°C. Geochim. Cosmochim. Acta 129, 125–145.

Sverjensky, D., Daniel, I., Brovarone, A.V., 2020. The changing character of carbon in fluids with pressure: organic geochemistry of Earth's upper mantle fluids. In: Geophysical Monograph Series. John Wiley and Sons Inc, pp. 259–269.

Syracuse, E.M., van Keken, P.E., Abers, G.A., Suetsugu, D., Bina, C., Inoue, T., Wiens, D., Jellinek, M., 2010. The global range of subduction zone thermal models. Phys. Earth Planet. Inter. 183 (1–2), 73–90.

Tao, R., Zhang, L., Tian, M., Zhu, J., Liu, X., Liu, J., Höfer, H.E., Stagno, V., Fei, Y., 2018. Formation of abiotic hydrocarbon from reduction of carbonate in subduction zones: Constraints from petrological observation and experimental simulation. Geochim. Cosmochim. Acta 239, 390–408.

Van Keken, P.E., Kiefer, B., Peacock, S.M., 2002. High-resolution models of subduction zones: Implications for mineral dehydration reactions and the transport of water into the deep mantle. Geochem. Geophys. Geosyst. 3 (10).

Vitale Brovarone, A., Martinez, I., Elmaleh, A., Compagnoni, R., Chaduteau, C., Ferraris, C., Esteve, I., 2017. Massive production of abiotic methane during subduction evidenced in metamorphosed ophicarbonates from the Italian Alps. Nat. Commun. 8, 1–13.

Vitale Brovarone, A., Sverjensky, D.A., Piccoli, F., Ressico, F., Giovannelli, D., Daniel, I., 2020. Subduction hides high-pressure sources of energy that may feed the deep subsurface biosphere. Nat. Commun. 11 (1), 1–11.

Wang, C., Tao, R., Walters, J.B., Höfer, H.E., Zhang, L., 2022. Favorable P–T–fO2 conditions for abiotic CH4 production in subducted oceanic crusts: A comparison between CH4-bearing ultrahigh- and CO2-bearing high-pressure eclogite. Geochim. Cosmochim. Acta 336, 269–290.

Wolery, T.J., 1992. EQ3/6, a Software Package for Geochemical Modeling of Aqueous Systems: Package Overview and Installation Guide (Version 7.0).
Zhang, C., Duan, Z., 2010. GFluid: an excel spreadsheet for investigating C-O-H fluid composition under high temperatures and pressures. Comput. Geosci. 36 (4), 569–572.
Zhu, J., Zhang, L., Tao, R., Fei, Y., 2020. The formation of graphite-rich eclogite vein in S. W. Tianshan (China) and its implication for deep carbon cycling in subduction zone. Chem. Geol. 533.